



Contents lists available at ScienceDirect

Bioorganic & Medicinal Chemistry

journal homepage: www.elsevier.com/locate/bmc

Pharmacophore requirements for HIV-1 reverse transcriptase inhibitors that selectively “Freeze” the pre-translocated complex during the polymerization catalytic cycle

Cyrus M. Lacbay^a, Michael Menni^b, Jean A. Bernatchez^b, Matthias Götte^{c,d}, Youla S. Tsantrizos^{a,b,*}

^a Department of Chemistry, McGill University, 801 Sherbrooke Street West, Montreal, Quebec H3A 0B8, Canada

^b Department of Biochemistry, McGill University, 3655 Sir William Osler Promenade, Montreal, Quebec H3G1Y6, Canada

^c Department of Medical Microbiology and Immunology, University of Alberta, 6-020 Katz Group Centre, Edmonton, Alberta T6G 2E1, Canada

^d Department of Microbiology and Immunology, McGill University, 3775 University Street, Montreal, Quebec H3A 2B4, Canada

ARTICLE INFO

Article history:

Received 18 December 2017

Revised 6 February 2018

Accepted 13 February 2018

Available online xxx

Keywords:

HIV-1 RT

Pyrimidinol carboxylic acids

Pre-translocated complex

Pyrophosphate mimics

ABSTRACT

Reverse transcriptase (RT) is responsible for replicating the HIV-1 genome and is a validated therapeutic target for the treatment of HIV infections. During each cycle of the RT-catalyzed DNA polymerization process, inorganic pyrophosphate is released as the by-product of nucleotide incorporation. Small molecules were identified that act as bioisosteres of pyrophosphate and can selectively freeze the catalytic cycle of HIV-1 RT at the pre-translocated stage of the DNA- or RNA-template-primer-enzyme complex.

© 2018 Elsevier Ltd. All rights reserved.

1. Introduction

Structural bioisosteres of pyrophosphate (**1**, PPI) include poly-oxygenated compounds, such as the natural product foscarnet (**2**; PFA), the malonate derivative **3** [2-(2-(4-chlorophenyl)hydrazono)-malonic acid; CPHM] and α,γ -diketo acids (**4**; DKA)¹ (Fig. 1). All of these compounds presumably bind to the active site of nucleic acid processing enzymes *via* metal-mediated interactions, blocking their catalytic function. A number of clinically validated human therapeutics, such as those targeting the virally-encoded HIV-1 integrase, are based on pharmacophores that mimic the pyrophosphate-metal interactions, characterizing the binding of the natural substrates. This class of compounds includes the approved drugs raltegravir (**5**)² and dolutegravir (**6**)³ as well as those currently under clinical development (**7** and **8**)⁴ (Fig. 1). Additionally, a number of exploratory compounds targeting other nucleic acid process-

ing enzymes, such as the HIV-1 RT^{5,6,7} and RNase H,^{8,9} and HCV NS5B RNA-dependent RNA polymerase,^{10,11} have been reported. However, drug design based on pharmacophores that mimic the molecular recognition elements of pyrophosphate (**1**) is a very challenging field of research, particularly when it comes to optimizing the target selectivity. For example, exploratory compounds such as **9a–c** and **10–13** (Fig. 2) inhibit various nucleic acid processing enzymes, but often with a very narrow window of selectivity. For example, analog **9c** was reported to be almost equipotent in inhibiting HCV NS5B and HIV-1 RT polymerase (IC₅₀ values of 29 μ M and 23 μ M, respectively),^{1b} and only a very minor difference in potency (~2-fold) was observed for analogs **11^{8b}** and **13^{8d}** in inhibiting HIV-1 RT vs HIV-1 RNase H or HIV-1 integrase.

These compounds all share a common structural feature, a metal-binding pharmacophore that mimics the interactions of pyrophosphate. Therefore, it is reasonable to assume that their binding in the active site of each enzyme is mediated by coordination to the divalent cations, which act as co-factors of all nucleic acid processing enzymes.¹² Experimental evidence may not be available for all enzymes; however, Mg²⁺ ions are the most likely physiologically relevant co-factors.¹³ Although neither direct comparison of the absolute potency values (IC₅₀) nor clear conclusions on structure-activity relationship (SAR) can be based on literature data (*i.e.* reported by different research groups using different

Abbreviations: HIV-1, human immunodeficiency virus type 1; RT, reverse transcriptase; PPI, inorganic pyrophosphate; NTP, nucleoside triphosphate; NDP, nucleoside diphosphate; PFA, phosphonoformic acid, foscarnet; RNase H, ribonuclease H; CPHM, [2-(2-(4-chlorophenyl)hydrazono)malonic acid; SAR, structure-activity relationship; HCV, hepatitis C virus.

* Corresponding author at: Department of Chemistry, McGill University, 801 Sherbrooke Street West, Montreal, Quebec H3A 0B8, Canada.

E-mail address: youla.tsantrizos@mcgill.ca (Y.S. Tsantrizos).

<https://doi.org/10.1016/j.bmc.2018.02.017>

0968-0896/© 2018 Elsevier Ltd. All rights reserved.

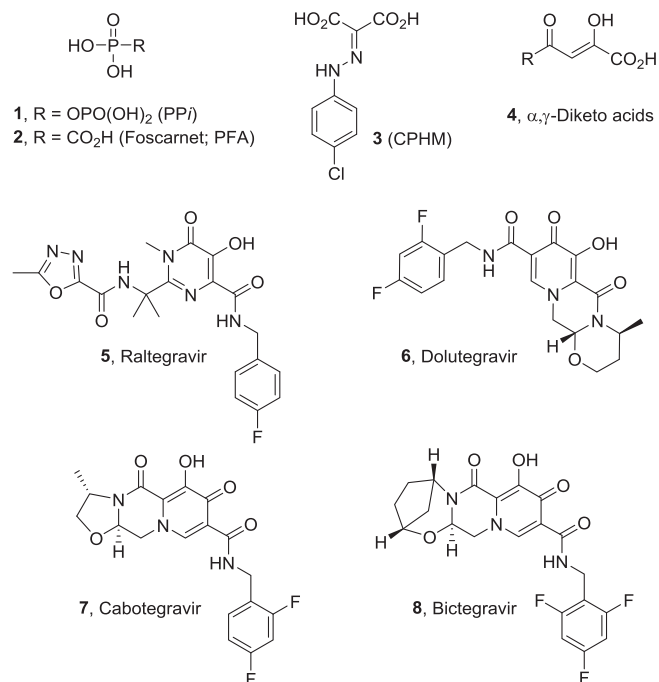


Fig. 1. Examples of biologically active compounds characterized by a metal-binding pharmacophore that mimics pyrophosphate (PPi; **1**) and are inhibitors of a nucleic acid processing enzyme. Analogs **5–8** are clinically validated inhibitors of HIV-1 integrase.

assay conditions), in a general sense, the reported literature data suggest that small structural modifications around the key pharmacophore moiety can modulate the target selectivity.

As part of our on-going investigations into the catalytic details associated with the function of HIV-1 reverse transcriptase (RT), we set out to design inhibitors that are chemically stable and can differentially block specific steps in the catalytic cycle of this enzyme. Previously, fosfarnet (**2**)^{5b,6c} and the malonate derivative **3**¹⁴ were identified as inhibitors of HIV-1 RT that selectively block the DNA polymerization cycle at the stage of the pre-translocated complex. However, both of these compounds suffer from poor

chemical and biopharmaceutical properties. In contrast, the α -carboxy nucleoside phosphate analog **14**,¹⁵ the pyridoindolone derivative **15**¹⁶ and benzofuropyridinone analog **16**¹⁷ inhibit RT by freezing the template-primer-enzyme complex at the post-translocated stage (Fig. 3). Herein, we report the identification of pyrimidinol carboxylic acid derivatives that inhibit HIV-1 RT with a mechanism similar to that observed with compounds **2** and **3**, by freezing the template (DNA or RNA)-primer-DNA polymerase pre-translocated complex. Although the pyrimidinol carboxylate can exist in two tautomeric forms (*i.e.* the dihydroxy and pyrimidinone), both are capable of chelating two Mg²⁺ cations in the active site of the enzyme. This chemotype imparts far superior drug-like properties as opposed to the metal-binding pharmacophores of inhibitors **2** and **3**.

2. Chemistry

Several protocols have been previously reported for the synthesis of aryl substituted pyrimidinol carboxylic acid derivatives (Scheme 1).^{1b,18} Initially, condensation of the amidine **18** with the fumarate reagent **19** (prepared from the *t*-butyl methyl oxalate **17**) was reported to provide access to C-2 alkyl- and aryl-substituted analogs in good to excellent yield (Scheme 1a).^{18a} However, fumarate **19** was also found to be chemically unstable and deprotection of the benzyl- and tert-butyl groups of the cyclized product **20** often required separate reactions, making the overall synthesis fairly lengthy. An alternative approach involved starting from nitrile **21**, which was first converted to the *N*-hydroxy amidine **22** and then condensed with dimethylacetylene dicarboxylate (DMAD; **23**) via a Michael-type reaction, to give intermediate **24** (Scheme 1b). Thermal dissociation of **24** at high temperatures (typically 130–140 °C) and re-Association to intermediate **25**, was reported to give the desired pyrimidinone ester **26** in low to modest yield (Scheme 1b).^{18b,18c} In-depth mechanistic investigations on the conversion of **24–26** proposed that a thermally induced homolytic N–O bond cleavage led to the formation of a radical polar pair that has a strong preference for recombination.¹⁹ Additionally, a more recent study showed that metal cations [*e.g.* Cu(I)/Cu(II) or Fe(II)] could significantly improve the outcome of this reaction, presumably by reducing the energy of the transition state through a single

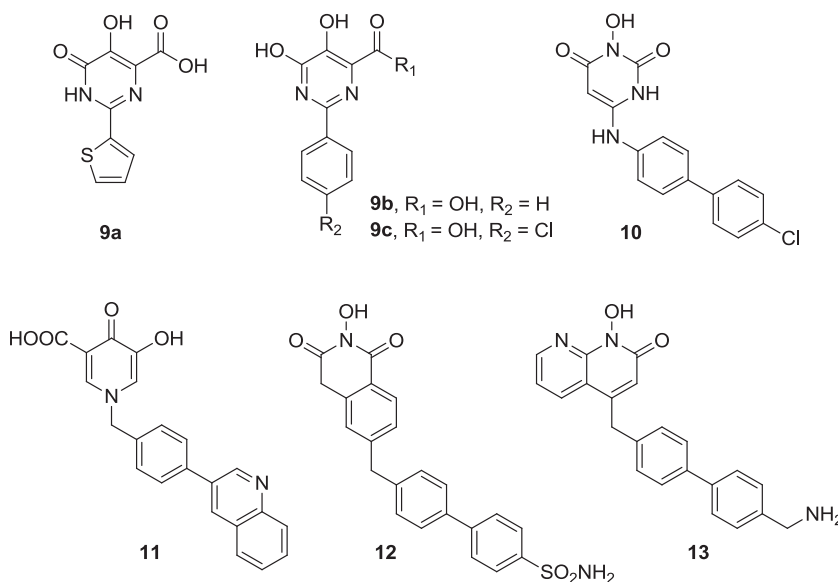


Fig. 2. Examples of exploratory compounds characterized by a metal-binding pharmacophore that inhibit various nucleic acid processing enzymes.

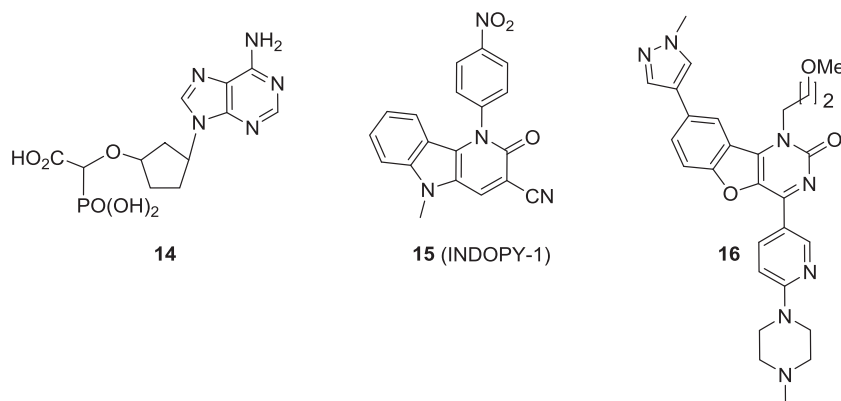
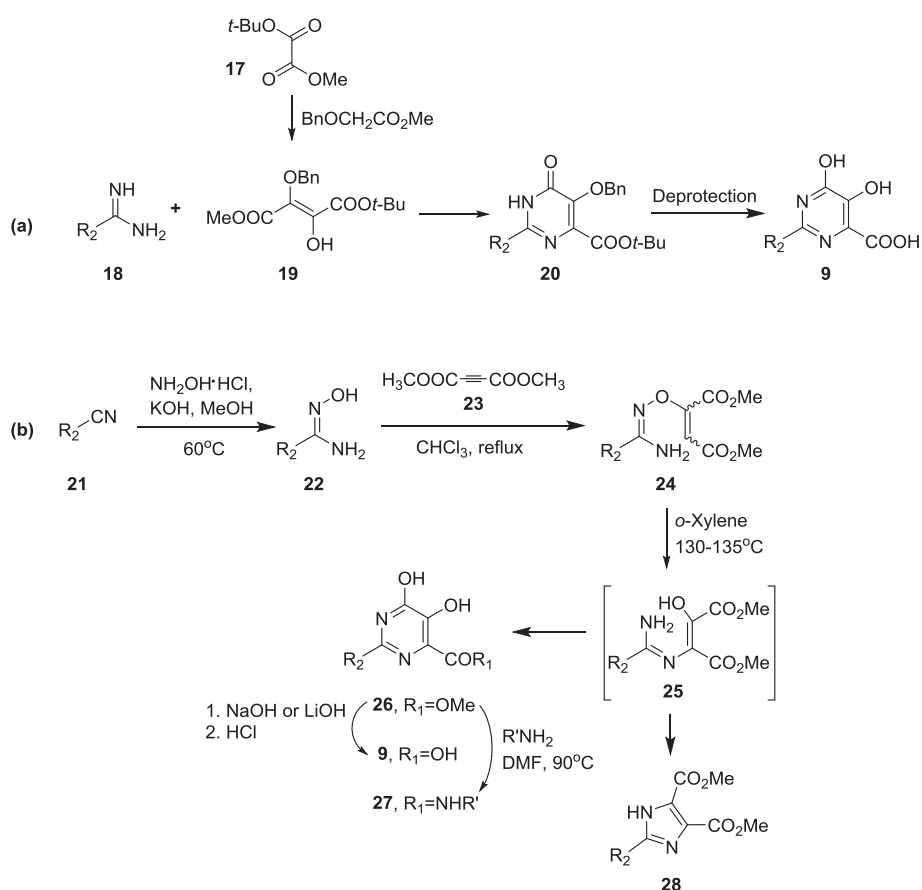


Fig. 3. Examples of compounds that inhibit the HIV-1 RT polymerase by specifically freezing the template-primer-enzyme complex at the post-translocated stage.



Scheme 1. Two synthetic routes, (a) and (b), that can be used to prepare substituted pyrimidinol carboxylic acid derivatives. Route (b) was used for the synthesis of analogs with R_2 fragments selected from **a–o** (Table 1).

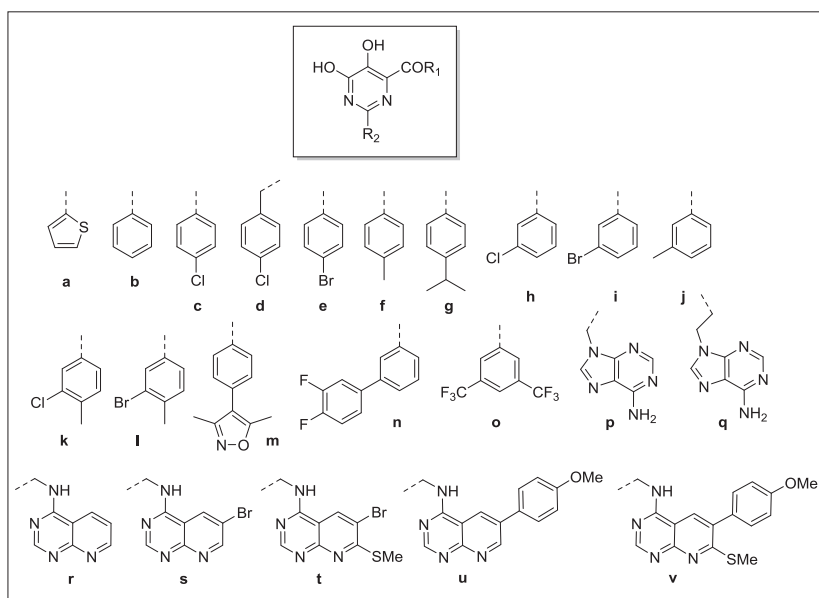
electron transfer reduction mechanism.²⁰ Although the best catalysts identified in these studies were the dibromo- and dichloro-(1,10-phenanthroline)/Cu(II) salts, other more readily available copper sources (e.g. CuBr) could also improve the outcome of this reaction.

We synthesized a small library of pyrimidinol carboxylic acid derivatives (analogs **9d–o**; Table 1), including some previously reported compounds (i.e. analogs **9a–c**),^{1b,10} following Scheme 1b with minor modifications. For example, we opted to use the more common copper additive, CuBr. However, we found that the solubility of ester intermediates **26** in organic solvents was usually very poor, making removal of this catalyst extremely

difficult. Consequently, CuBr was used only for the most challenging reactions, such as the preparation of adenine derivatives **32a** and **32b** (Scheme 2); the majority of intermediates **26** (Scheme 1) were easily purified by a simple trituration.

The synthesis of the adenine-based compounds (analogs **9p** and **9q**; Table 1) was achieved via the amidoxime intermediates **29** (Scheme 2), which were synthesized from known nitrile intermediates.²¹ Although reaction of **29** with DMAD to give the Michael adduct **30** proceeded in good yields (in the presence of triethylamine in DMSO), the thermal rearrangement of **30** (via the presumed intermediate **31**) in xylenes at 130 °C led mostly to

Table 1
Representative examples of a pyrimidinol carboxylate-based library of HIV-1 RT polymerase inhibitors.



Compound	R ₁	R ₂	IC ₅₀ RT Pol (μM)	Compound	R ₁	R ₂	IC ₅₀ RT Pol (μM) ^α
2	–	–	0.8 ± 0.2	9l	OH	l	1.4 ± 0.2
3	–	–	1.5 ± 0.2	9m	OH	m	>100
9a10	OH	a	46 ± 3.5	9n	OH	n	>100
9b1b	OH	b	>100	9o	OH	o	20 ± 0.6
9c1b	OH	c	4.5 ± 0.5	9p	OH	p	>100
9d	OH	d	97 ± 13	9q	OH	q	41 ± 8
9e	OH	e	2.8 ± 0.2	9r	OH	r	65 ± 5.8
9f	OH	f	6.3 ± 0.4	9s	OH	s	49 ± 5.4
9g	OH	g	22 ± 1.3	9t	OH	t	>100
9h	OH	h	18 ± 2.6	9u	OH	u	25 ± 16 ^β
9i	OH	i	14 ± 3.6	9v	OH	v	62 ± 20 ^β
9j	OH	j	49 ± 10	26l	OMe	l	>100
9k	OH	k	1.6 ± 0.2	27l	NHMe	l	>100

Analogs were synthesized as follows: **9a–o**, **26l**, and **27l** (Scheme 1b); **9p–q** (Scheme 2); and **9r–v** (Scheme 3).

^α IC₅₀ values are the average of at least three independent determinations using a DNA synthesis assay catalyzed by the HIV-1 RT polymerase.

^β The high variability observed with these compounds may suggest aggregation in the assay buffer at high concentrations leading to artefact. However, since neither their potency nor mechanism of action were of interest in our present study, we did not explore these compounds any further.

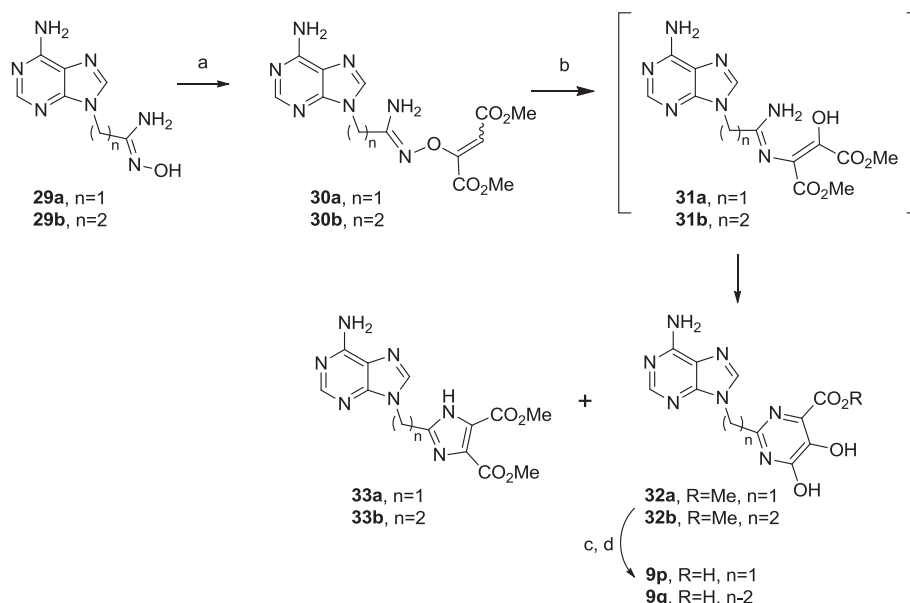
decomposition. However, in the presence of CuBr (50 mol%)²⁰ a reasonable yield of the desired product **32** was obtained within 30 min at the same temperature, in addition to small amounts of the expected imidazole side product **33** (identification and quantification of **33** was based on its LC-MS data). It is noteworthy that due to the high polarity of the adenine-based analogs, the purification was very challenging, accounting (*in part*) for the low isolated yields (~30%). All of these reaction mixtures were purified by HPLC using C₁₈ reversed phase chromatography. Finally, in order to probe the impact of the carboxylate anion in the potency of our compounds, we also tested the ester analog **26l** and its corresponding *N*-methylamide derivative **27l** (Table 1).

Previously, we reported the modular synthesis of pyrido[2,3-*d*]pyrimidines (Scheme 3; **34**), a scaffold that can serve as a purine mimic.⁵ We identified several analogs with a bisphosphonate anchor that inhibit the HIV-1 RT-catalyzed DNA synthesis.⁵ However, at that time the exact mechanism of inhibition was not determined. As a follow-up to these investigations, in the present study, we also explored non-bisphosphonate derivatives having the pyrimidinol carboxylate moiety as the metal-binding motif (e.g. Table 1; compounds **9r–9v**). Synthesis of these compounds was initiated from the pyrimidinone intermediate **36**, which was prepared starting from either the 4-amino fragment **34**⁵ or directly

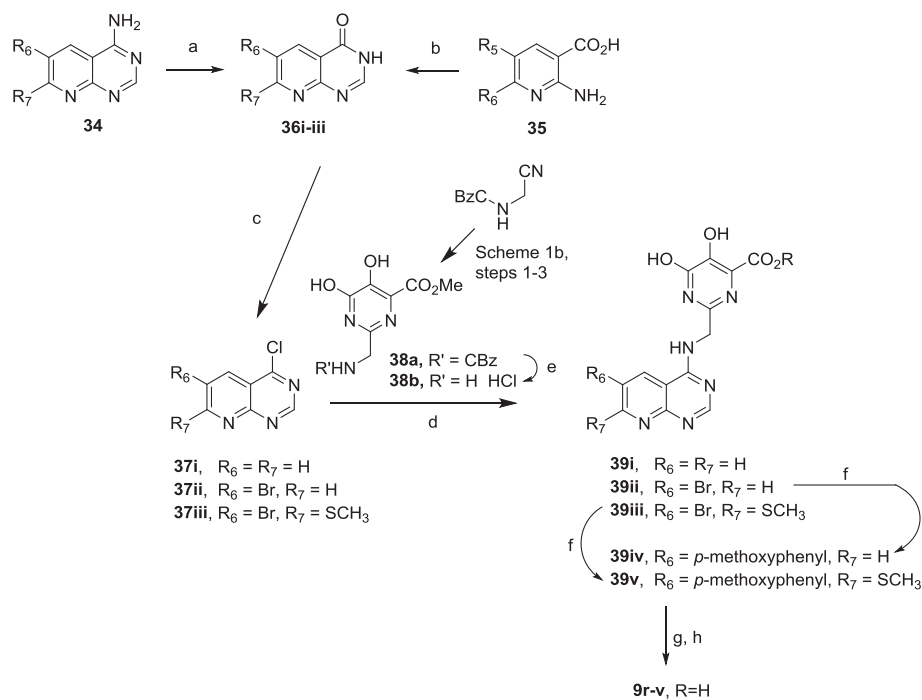
from the substituted pyridine **35** (Scheme 3). Treatment of **36** with POCl₃ afforded the 4-chloropyridopyrimidine intermediate **37**, which was reacted with amine **38b** under S_NAr conditions to give **39**. The precursor of **38b** (fragment **38a**) was synthesized from the CBz-protected 2-aminoacetonitrile following the same protocol as in Scheme 1b. In cases where the R₆ moiety of **39** was a bromide, this intermediate was also subjected to Pd-catalyzed cross-coupling reactions in order to further increase the structural diversity of our library by introducing a variety of aryl or heteroaryl groups (e.g. analogs **9u** and **9v**; Table 1). The final inhibitors were obtained after hydrolysis of the methyl ester under standard basic conditions. Representative analogs from our library are shown in Table 1 (e.g. analogs **9r–v**).

3. Results and discussion

“Translocation” is a key step that occurs during the DNA polymerization process catalyzed by the HIV-1 RT polymerase (Fig. 4). This step refers primarily to the translocation of the elongated primer terminus to the so-called priming site (P-site), which frees the nucleotide binding site (N-site) for binding of the next substrate monomer, the deoxynucleoside triphosphate (dNTP;



Scheme 2. Synthesis of adenine-based compounds (e.g. **9p–q**). Conditions: (a) DMAD, Et₃N (~0.1–1.0 eq), DMSO, rt, 4–16 h, 50–80%; (b) CuBr (50 mol%), dry dioxane, 130 °C, under Ar atmosphere, 30 min, ~30%; (c) LiOH, MeOH:THF:H₂O (2:2:1), 50–60 °C, 4–12 h; (d) aq. HCl (70–80%).



Scheme 3. Synthesis of pyridopyrimidine-based compounds (e.g. **9r–v**). Conditions: (a) Methanesulfonic acid/H₂O, 100 °C, 1 h, 60–94%; (b) Formamide, 145 °C, 20–48 h, 58–68%; (c) POCl₃, toluene, pyridine, 115–180 °C, ~2h, 30–65%; (d) DMSO/dioxane, Et₃N, under Ar atmosphere, 100 °C, 1 h, ~50–70%; (e) H₂, Pd/C, 6 N HCl, 76%; (f) 4-methoxyphenylboronic acid, Pd(PPh₃)₄, KF, MeOH/dioxane (4:1), 120 °C, ~55%; (g) LiOH, MeOH:THF:H₂O (2:2:1), 50–60 °C; (h) aq. HCl.

Fig. 4). Previous studies suggested that the HIV-1 RT polymerase establishes a dynamic equilibrium between the pre- and the post-translocation conformations. This equilibrium depends on several parameters including the sequence of the nucleic acid substrate. We have previously shown that foscarnet acts preferentially on primer/template sequences that show a bias towards pre-translocation^{6b}; *i.e.* hot spots for inhibition were identified at primer/template sequences that promote the formation of the pre-translocated state. Foscarnet-mediated inhibition of polymerization leads to the accumulation of position +3 and +16

oligonucleotide fragments, characterizing the “freezing” of the pre-translocated state. Therefore, site-specific foot-printing experiments can conclusively differentiate the selective trapping of the two translocation states by various inhibitors.⁶

In the course of our current studies, we prepared a library of HIV-1 RT inhibitors having the pyrimidinol carboxylate bioisostere as the key pharmacophore. This is a privileged drug-like structural motif, which mimics pyrophosphate (**1**) and has been successfully employed in drug discovery. Representative examples from our library are shown in Table 1. All analogs were tested in parallel

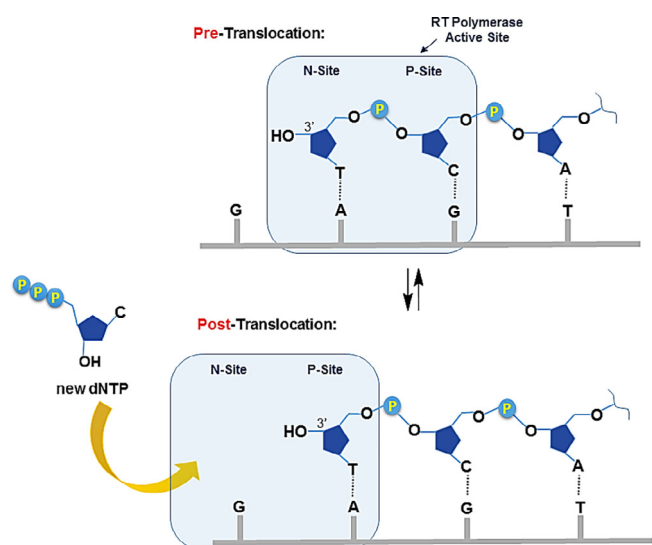


Fig. 4. Representation of the translocation step in the DNA polymerization cycle catalyzed by HIV-1 RT polymerase.

with literature compounds (as positive controls) that are known to specifically block the pre-translocation (e.g. compound **2**) and post-translocation complex (e.g. **15**) of the HIV-1 RT polymerization cycle.^{6,14–17} The IC_{50} values of all our compounds (Table 1) were determined using a previously reported gel-based DNA synthesis assay.¹⁴

DNA synthesis inhibition data (IC_{50} values) indicated that the unsubstituted phenyl compound **9b** did not exhibit any significant activity at the highest concentration tested of 100 μ M, using our previously reported DNA polymerization gel-based assay.¹⁴ However, analogs with a chloro, bromo, or methyl substituent at the *para*- position of the C-2 phenyl (i.e. Table 1; analogs **9c**, **9e**, and **9f**) exhibited potencies in the 3–6 μ M range. Generally, *meta* substitution was less favorable than the corresponding *para*-substitution; for example, 4-, 5-, and 8-fold decrease in potency was observed between the *para*- and *meta*- substituents for the chloro (**9c** vs **9h**), bromo (**9e** vs **9i**), and methyl (**9f** vs **9j**) derivatives, respectively (Table 1). Incorporation of larger substituents, either at the *meta*- or the *para*-positions, results in modest loss of potency (e.g. 2- to 4-fold) for relatively small substitution changes (e.g. **9g** vs **9f**) to very significant loss of potency for larger substituents (e.g. analogs such as **9m** and **9n** vs **9f**), suggesting a limited volume of space in the binding pocket of these inhibitors. This observation is consistent with the small volume of space that would be required for the binding of the pyrophosphate (**1**) by-product released during the catalytic cycle (i.e. before **1** is expelled from the active site). In contrast, much larger molecules, such as compounds **14** and **15**, would require a much larger binding pocket and could potentially occupy the nucleotide binding site (N-site), thus freezing the catalytic cycle at the post-translocated stage (Fig. 4). It is noteworthy that although we are currently assuming that all of our small (in molecular size) analogs **9** are adopting the same binding mode, the possibility of multiple binding modes cannot be ruled-out without further investigations. Introduction of a methylene linker between the metal-binding pharmacophore and the aromatic ring (e.g. **9c** vs **9d**) also resulted in a significant loss of potency (~19-fold; Table 1), in addition to loss in selectivity in blocking the pre- vs post-translocation step of the enzyme (Fig. 6). These observations are likely due to both the increased molecular size and the higher conformational flexibility of the side chain. Replacement of the phenyl moiety with monocyclic heterocycle, such as a thiophene (e.g. **9a**) or a bicyclic heterocycle, such as adenine or

pyridopyrimidine (e.g. **9q** or **9r**) did not offer any advantages in terms of potency. Di-substituted inhibitors **9k** and **9l** were the best analogs identified in this library of compounds, with IC_{50} values in the 1–2 μ M range. The potency of these compounds seems to be highly dependent on the carboxylate anion, as the corresponding ester and amide of **9l** (i.e. **26l** and **27l**, respectively) were found to be inactive at the highest concentration tested of 100 μ M (a much larger number of non-carboxylate derivatives would need to be evaluated in order to confirm this observation).

Our gel-based DNA synthesis assay is based on quantitative analysis of the DNA primer extension by the HIV-1 RT polymerase, however, it is also sensitive to the mechanistic details of the inhibition.¹⁴ Specific pausing patterns associated with pre- and post-translocation inhibition can be observed using this assay.^{6b,14} Consistent with our above hypothesis, the most potent of our small molecular size pyrimidinol carboxylic acids also exhibited the characteristic profile of a pre-translocation inhibitor (Fig. 5). For example, inhibitors **9k** and **9l** showed clear polymerization pausing after the incorporation of three and sixteen monomer units to the 3'-end of the primer (Fig. 5). Similar results were observed with foscarnet (**2**), as well as all other analogs having a small substituted phenyl side chain (including **9c**, **9e**, **9h** and **9i**). Interestingly, the addition of a single methylene linker between the metal-binding pyrimidinol carboxylic acids moiety and the side chain is sufficient to induce significant loss in potency and selectivity in “freezing” the pre-translocated stage of RT (e.g. **9c** vs **9d**).

Additionally, we used site-specific foot-printing experiments to probe the mechanism of action of our best compounds.^{6b,14} Literature compounds **2** and **15** were tested in parallel as the positive controls, in order to confirm selective freezing of the primer-template-enzyme complexes at the pre-translocation and post-translocation stages, respectively (Fig. 6). Consistent with the pausing data observed in the DNA polymerization assay (Fig. 5), cleavage fragments corresponding to pre-translocated complex were observed in the foot-printing assay with the small pyrimidinol carboxylate inhibitors **9l** and **9i** (Fig. 6; lanes 9 and 10, respectively), as well as the control inhibitor **2** (lane 4).

Previously, we also explored bisphosphonate bioisosteres of pyrophosphate as potential inhibitors of HIV-1 RT polymerase.⁵ In this study, we compared the mechanism of action of analogs **40** and **41** (Fig. 6) to those of structurally related members of our pyrimidinol carboxylic acids (e.g. analogs **9i** compared to compound **41**). Analog **9i** and **41** have structurally and electronically distinct metal-binding motifs, but bear the exact same side chain, a *meta*-bromophenyl group. As shown in Fig. 6, the pausing patterns of **9i** (lane 10) and **41** (lane 6) are clearly the same, which further supports our hypothesis that irrespective of the metal-binding pharmacophore, only inhibitors with small side chains (e.g. **41**, but not **40**; Fig. 3, lanes 6 and 5, respectively) can bind to the pyrophosphate binding site and selectively freeze the catalytic cycle at the pre-translocated stage. These observations are in clear contrast to the fragmentation pattern observed with the post-translocation inhibitor **15** (Fig. 3; lane 3). A dose-dependent inhibition that specifically blocked the pre-translocation complex of HIV-1 RT was also observed with our most potent inhibitors **9k** and **9l**. It is noteworthy that most analogs with a large side chain did not induce 50% inhibition of the polymerase enzyme at concentrations below 50 μ M (Table 1). The few analogs that gave an IC_{50} of approximately 20 μ M (e.g. **9o** and **9u**) did not show any clear pausing pattern in the DNA polymerization assay, nor any specific fragmentation pattern in the foot-printing assay (for an example refer to the Supporting Information, SI Fig. 1), suggesting that these compounds have a mixed or non-specific mode of inhibition. It should be noted that high micromolar IC_{50} values can be very unreliable as experimental artefacts in a functional assay at high

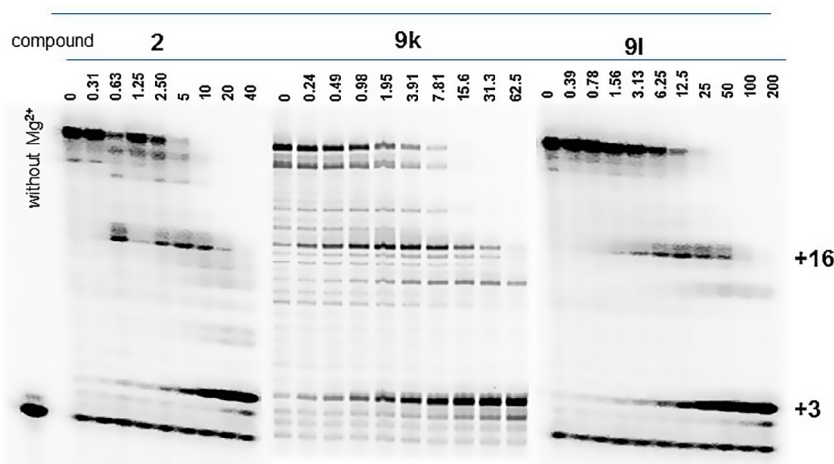


Fig. 5. Inhibition of HIV-1 RT DNA synthesis by compounds **2**, **9k** and **9l**. All three compounds induced identical pausing patterns in DNA synthesis, predominantly at an extension of +3 and +16 monomer units from the 3'-end of the primer.

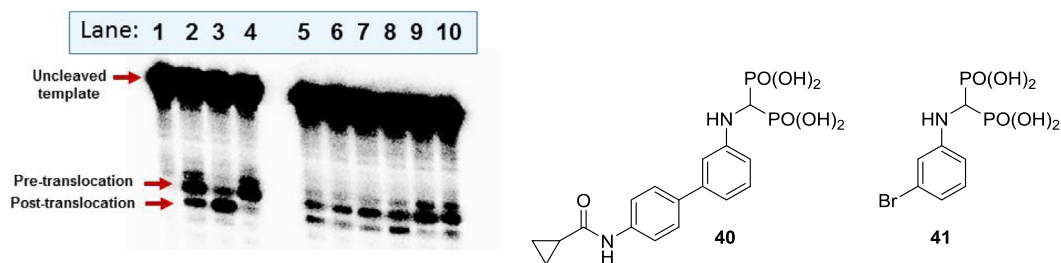


Fig. 6. Site-specific foot-printing assay data. All experiments were run in the presence of Fe^{2+} as previously reported with the exception of the control in lane 1, which was run without the metal ions. Screening was performed at a fixed concentration; inhibitor **15** was tested at 10 μM and all other compounds were tested at 100 μM . Lane 2: control experiments without inhibitor; lane 3: inhibitor **15**; lane 4: inhibitor **2**; lane 5: bisphosphonate inhibitor **40**; lane 6: bisphosphonate inhibitor **41**; lane 7: inhibitor **9h**; lane 8: inhibitor **9d**; lane 9: inhibitor **9l**; lane 10: inhibitor **9i**.

concentrations of a compound can contribute to the observed potency and mislead SAR studies. Lipophilicity-dependent aggregation of moderately (or poorly) hydrophilic compounds is the most common factor responsible for false experimental data and can affect both *in vitro* and cell-based assays.²² There are other numerous ways by which an aromatic compound may appear to inhibit RT DNA polymerization in an assay (e.g. intercalation into the oligonucleotide substrate) and consequently, unraveling the details of the mechanism of action of these compounds will require further investigations.

To gain some insight into the selectivity of our compounds in targeting the RT polymerase vs the RNase H catalytic domain, representative analogs were also tested in our RNase H assay using the natural product β -thujaplicinol (**42**; Fig. 8) as the positive control (Table 2).²³ Our most potent RT polymerase inhibitors, **9k** and **9l**, were >10-fold less potent in our RNase H inhibition assay and ~30-fold less potent than β -thujaplicinol (**42**). In contrast, some of our pyridopyrimidine-based compounds (e.g. **9u** and **9v**; Table 2), exhibited reversed selectivity, with potency close to that of β -thujaplicinol in inhibiting RNase H (Table 2). Finally, we also evaluated our most potent inhibitor, compound **9l**, for its ability to block the catalytic function of the K65R, E89K and M184V HIV-1 RT mutants (Fig. 7). A negligible difference in potency between these mutants and the wild-type RT enzyme was observed; <2-fold difference in IC_{50} with K65R and M184V, and only a 2.7-fold difference observed with the E89K mutant. Therefore, the activity profile and mechanism of action of our best pyrimidinol carboxylates appear to be comparable to that of foscarnet

(**2**)^{6b,14}; however, these analogs are far more drug-like and thus, better leads for drug discovery.

In summary, we explored the mechanistic details of HIV-1 RT inhibition by pyrimidinol carboxylic acid derivatives and identified some interesting structural elements that may be further explored in order to develop *bona fide* HIV-1 RT polymerase *active site* inhibitors that selectively freeze the catalytic cycle at the pre-translocated complex (Fig. 4). Our preliminary SAR studies suggest that small substituents attached to the metal-coordinating pyrimidinol carboxylate pharmacophore may allow binding of these molecules to the sub-pocket of the active site typically occupied by the inorganic pyrophosphate (**1**) by-product released during the catalytic cycle. This conclusion is consistent with the small volume of space around the RT-bound foscarnet in the previously reported ternary complex of RT/DNA/foscarnet.^{6c} At this time, the exact mode of binding of our best compounds to the RT-primer-template complex is unclear. Although we contemplated probing the binding interactions of our inhibitors by docking these compounds to the ternary complex of RT/DNA/foscarnet,^{6c} given the protein plasticity and the conformational complexity of this system, we believe that *in silico* studies would be unreliable for guiding structure-based drug design and consequently, we are focusing our current efforts on crystallographic studies.

The pyrimidinol carboxylate pharmacophore (e.g. **9a–c**) has been previously explored in the design of HCV NS5B RNA-dependent RNA polymerase inhibitors and compound **9c** was shown to also inhibit HIV-1 RT.^{1b} However, detailed mechanistic investigations probing the specific mode of action of this

Table 2
Selectivity data in inhibiting HIV-1 RT polymerase vs RNase H by pyrimidinol carboxylic acid compounds.

Compound	R ₁	R ₂	IC ₅₀ RT Pol (μM)	IC ₅₀ RT RNase H (μM)
40	–	–	>50 ^a	0.8 ± 0.3
9k	OH	k	1.6 ± 0.2	25.0 ± 5.3
9l	OH	l	1.4 ± 0.2	23.0 ± 5.1
9u	OH	u	25 ± 16 ^b	1.5 ± 0.1
9v	OH	v	62 ± 20 ^b	2.0 ± 1.3

IC₅₀ values are average of at least three determinations.

^a IC₅₀ value reported by Budihas et al.²³

^b As mentioned in Table 1, at high concentrations of compound, aggregation may lead to artefacts. However, these compounds are clearly more potent inhibitors of the HIV-1 RNase H than the RT polymerase.

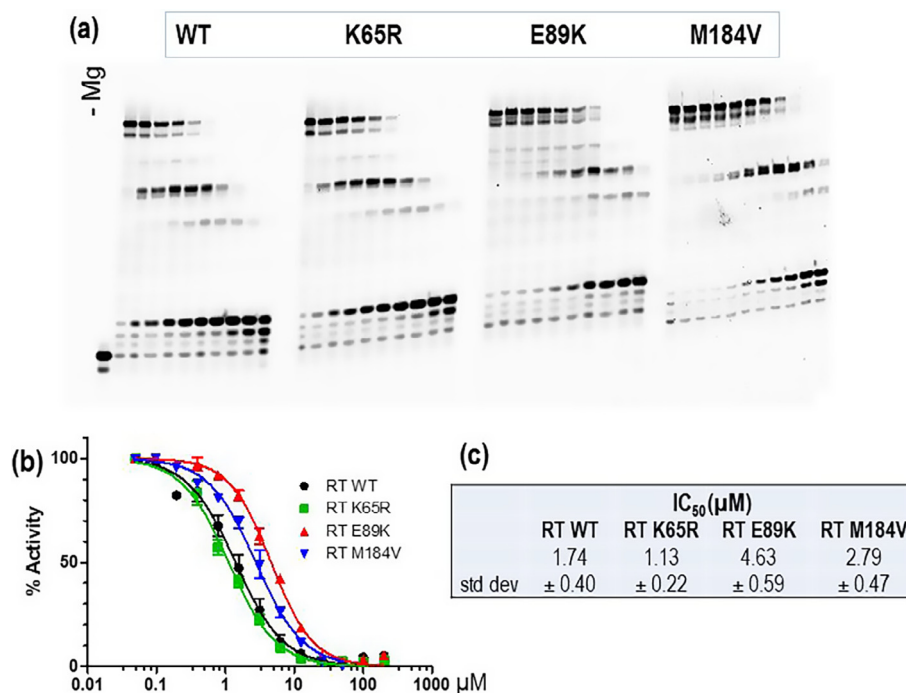


Fig. 7. Biological profiling of inhibitor **9L** in the HIV-1 RT polymerase assay with the wild type enzyme and the K65R, E89K and M184V mutants. (a) Inhibition of HIV-1 RT DNA synthesis indicating an identical pausing patterns in DNA synthesis, predominantly at an extension of +3 and +16 monomer units from the 3'-end of the primer. (b) Dose-dependent inhibition curves of the polymerase enzymes. (c) Tabulated data showing IC₅₀ values for the wild-type and mutants of the HIV-1 RT polymerase.

compound in inhibiting HIV-1 RT was not reported.^{1b} Other inhibitors of HIV-1 RT polymerase include the 4-dimethylamino-6-vinylpyrimidine **43** (DAVP-1; Fig. 8), initially presumed to be an active site inhibitor of the HIV-1 RT polymerase.²⁴ However, crystallographic studies revealed that this compound binds to a site adjacent to the polymerase active site. Therefore, the mode of action of **43** is more similar to that of an allosteric inhibitor, causing a conformational change of the enzyme-bound primer/template complex, thus interfering with the proper incorporation of the nucleotide substrate.^{7,25} Other chemotypes of HIV-1 RT and RNase H inhibitors include various metal-binding pharmacophores, (e.g. analogs **10–13**)⁸ and efforts in designing inhibitors that can distinguish between HIV-1 RT polymerase and RNase H have been reported.²⁶

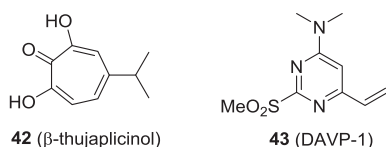


Fig. 8. Structures of the HIV-1 RNase H inhibitor β-thujaplicinol (**42**) and HIV-1 RT polymerase inhibitor, DAVP-1 (**43**).

4. Conclusions

In the absence of a cure for HIV, the quest for finding new therapeutic agents to combat this infection continues. Discovery of small molecule inhibitors that function with a novel mechanism of action may offer advantages over the current therapeutics in the treatment of drug-resistant HIV mutants. While it is not surprising that many metal-binding compounds may suffer from poor target selectivity in blocking the catalytic function of a nucleic acid processing enzyme, understanding the mechanistic details in each case can provide valuable insight in the design of potent and highly selective inhibitors for a specific biological target. In this report, we identified a series of pyrimidinol carboxylate-based inhibitors of the HIV-1 RT polymerase that specifically freeze the pre-translocated state of the enzyme's catalytic cycle. Our preliminary SAR studies provided some evidence on the structural requirements suitable in targeting the pre-translocated complex of the RT polymerase. It remains to be determined whether the presumed small volume of the pyrophosphate binding site will prevent the discovery of more potent HIV-1 RT polymerase inhibitors that exhibit high target selectivity. Nonetheless, these results provide a venue for the development of mechanistically distinct, true active site inhibitors of HIV-1 RT with potential therapeutic applications.

5. Experimental section

5.1. General procedures for characterization of compounds

All synthetic intermediates were purified by normal phase flash column chromatography on silica gel using a CombiFlash instrument and a solvent gradient from 5% EtOAc in hexanes to 100% EtOAc and then to 20% MeOH in EtOAc, unless otherwise indicated. During our library synthesis, the progress of most reactions was followed by TLC and/or LC-MS and most often intermediate building blocks were used in the subsequent step without purification and full characterization. However, in order to validate the protocols used for our library synthesis, key intermediates for select compounds were purified by chromatography and fully characterized by ^1H and ^{13}C NMR, as well as HRMS.

The homogeneity of all final inhibitors was confirmed to be $\geq 95\%$ by C_{18} reversed-phase HPLC. HPLC analysis was performed using a Waters ALLIANCE[®] instrument (e2695 with 2489 UV detector and 3100 mass spectrometer). Key final inhibitors were fully characterized by ^1H and ^{13}C NMR, and HRMS. Chemical shifts (δ) are reported in ppm relative to the internal deuterated solvent (^1H , ^{13}C) unless indicated otherwise. High resolution MS spectra of all final products were recorded using electrospray ionization ($\text{ESI}^{+/-}$) and Fourier transform ion cyclotron resonance mass analyzer (FTMS). For bromine-containing inhibitors (e.g. **9e**, **9i**, **9l**, **9s**, and **9t**), the reported HRMS data correspond to the calculated and observed ^{79}Br isotope; the ^{81}Br isotope, was also observed, but for simplicity, it is not reported.

5.2. Analytical HPLC method (homogeneity analysis using a Waters atlantis T3 C_{18} 5 μm column)

Solvent A: H_2O , 0.1% formic acid.

Solvent B: CH_3CN , 0.1% formic acid.

Mobile phase: linear gradient from 95%A and 5%B to 0%A and 100%B in 13 min.

5.3. General protocols for the synthesis of final inhibitors **9a–9o**

Synthetic methodologies were based on previously reported protocols with some modifications.^{1b,18b}

Step 1: Preparation of amidoxime intermediates **22a–o**

A 1.0 M solution of hydroxylamine hydrochloride in MeOH (2.0 eq) and a 1.0 M solution of KOH in MeOH (2.0 eq) were combined at 0 °C and stirred for ~ 30 min (slowly warming from 0 °C to rt). The potassium chloride salt formed was removed by filtration. The filtrate was added to the nitrile **21** [1.0 eq; the corresponding nitrile was either purchased from commercial source (analogs **21a–l** and **21o**), or synthesized starting from a commercial nitrile, which was further modified via a Suzuki coupling reaction using established methods (**21 m–n**)] and the mixture was heated at 60 °C for 17–24 h. MeOH was removed under vacuum and the residue was diluted with EtOAc, washed with brine, and the organic layer was concentrated. The product **22** was typically obtained in quantitative yield and $>90\%$ purity, and was used in the next step without further purification.

Step 2: Preparation of Michael adduct intermediates **24a–o**

Dimethylacetylene dicarboxylate (**23**, DMAD; 1.1 eq) was added dropwise to a solution of amidoxime **22** (1.0 eq) in CHCl_3 (1.3 mL per 1.0 mmol **22**) and the mixture was heated at 60 °C for 1–2 h. Chloroform was removed under vacuum and the crude residue

was usually used immediately in the next step (only in few cases, this intermediate needed to be purified by silica-gel column chromatography, using a gradient 5–50% EtOAc in hexanes). The conversion of intermediate **22–24** was monitored by TLC and/or LC-MS and usually the product **24** was used immediately in the next step. Intermediate **24** was typically obtained as a mixture of E/Z isomers (isolated yield was typically $\geq 70\%$).

Step 3: Preparation of the pyrimidinone esters **26a–o**

Intermediate **24** in *o*-xylenes (2.5 mL per 1.0 mmol **24**) was heated to 130–135 °C for 4–12 h and then cooled to rt (progress of the reaction was monitored by TLC or LC-MS). Methyl tert-butyl ether (MTBE) and MeOH (5.0 mL, 9:1 ratio) was added (with stirring) and the resulting slurry was cooled in an ice-bath for at least 30 min. The solid precipitate was collected via filtration, washed several times with MTBE:MeOH (9:1) and then dried under vacuum. The product was further purified by trituration, as necessary, to give **26** in 20–45% isolated yield.

Step 4: Final inhibitors **9a–9o**

Pyrimidinone carboxylate ester **26** (1.0 eq) and LiOH (3.0–10.0 eq) in MeOH/THF/ H_2O (2:2:1; ~ 8.0 mL per 0.1 mmol **26**) was stirred at 50–60 °C for 4–12 h. The mixture was concentrated under vacuum and acidified to pH 2–3 with 1 N HCl. The precipitate was filtered and dried under vacuum to give the final inhibitors **9** in 50% to quantitative isolated yield and high purity. Final products which did not meet the required purity for testing in biological assays (i.e. $\geq 95\%$ homogeneity, as determined by analytical C_{18} reversed phase HPLC and confirmed by ^1H NMR) were further purified by C_{18} reversed phase HPLC.

5.3.1. Compound characterization

5.3.1.1. 5,6-Dihydroxy-2-(thiophen-2-yl)pyrimidine-4-carboxylic acid (**9a**)^{10,11,27}. Pyrimidinone ester **26a**: Isolated as a light orange solid. ^1H NMR (500 MHz, DMSO-d_6) δ 13.21 (br_s, 1H), 10.50 (br_s, 1H), 7.99 (d, $J = 3.3$ Hz, 1H), 7.76 (dd, $J = 5.0, 0.9$ Hz, 1H), 7.17 (dd, $J = 5.0, 3.8$ Hz, 1H), 3.84 (s, 3H). MS [ESI^+] m/z : 253.1 [$\text{M} + \text{H}^+$]⁺.

Inhibitor **9a**: Isolated as a pale yellow solid. ^1H NMR (500 MHz, DMSO-d_6) δ 13.08 (br_s, 1H), 7.99 (dd, $J = 3.8, 0.9$ Hz, 1H), 7.76 (dd, $J = 5.0, 0.9$ Hz, 1H), 7.16 (dd, $J = 5.0, 3.8$ Hz, 1H). MS [ESI^-] m/z : 237.0 [$\text{M} - \text{H}^+$]⁻; ^1H NMR consistent with that reported in the literature.²⁷

5.3.1.2. 5,6-Dihydroxy-2-phenylpyrimidine-4-carboxylic acid (**9b**)^{1b,9}

Amidoxime **22b**: Isolated as a yellow oil. ^1H NMR (500 MHz, DMSO-d_6) δ 9.61 (s, 1H), 7.69 – 7.64 (m, 2H), 7.39 – 7.35 (m, 3H), 5.78 (br_s, 2H). MS [ESI^+] m/z : 137.1 [$\text{M} + \text{H}^+$]⁺.

Pyrimidinone ester **26b**: Isolated as a light orange solid. ^1H NMR (400 MHz, DMSO-d_6) δ 8.02–7.99 (m, 2H), 7.53 – 7.47 (m, 3H), 3.85 (s, 3H). MS [ESI^+] m/z : 247.1 [$\text{M} + \text{H}^+$]⁺.

Inhibitor **9b**: Isolated as a light peach solid. ^1H NMR (400 MHz, DMSO-d_6) δ 8.04 (d, $J = 8.0$, 2H), 7.56–7.45 (m, 3H). MS [ESI^-] m/z : 231.1 [$\text{M} - \text{H}^+$]⁻; ^1H NMR consistent with that reported in the literature.^{1b,9}

5.3.1.3. 2-(4-Chlorophenyl)-5,6-dihydroxypyrimidine-4-carboxylic acid (**9c**)^{1b,27}. Amidoxime **22c**: Isolated as a white solid. ^1H NMR (500 MHz, DMSO-d_6) δ 9.72 (s, 1H), 7.70–7.66 (m, 2H), 7.45–7.41 (m, 2H), 5.86 (br_s, 2H). MS [ESI^+] m/z : 171.3 [$\text{M} + \text{H}^+$]⁺.

Pyrimidinone ester **26c**: Isolated as orange solid. ^1H NMR (500 MHz, DMSO-d_6) δ 8.03 (d, $J = 8.7$ Hz, 2H), 7.57 (d, $J = 8.8$ Hz, 2H), 3.85 (s, 3H). MS [ESI^+] m/z : 281.1 [$\text{M} + \text{H}^+$]⁺.

Inhibitor **9c**: Isolated as off-white solid. ^1H NMR (500 MHz, DMSO-d_6) δ 8.07 (d, $J = 8.7$ Hz, 2H), 7.56 (d, $J = 8.7$ Hz, 2H). ^{13}C

NMR (126 MHz, DMSO- d_6) δ 169.0, 159.3, 148.3, 144.4, 135.4, 131.1, 129.0, 128.6, 128.2. HRMS [ESI⁻] calculated for C₁₁H₆ClN₂O₄ m/z , 265.00216; found 265.00220 [M - H⁺]⁻.

5.3.1.4. 2-(4-Chlorobenzyl)-5,6-dihydroxypyrimidine-4-carboxylic acid (**9d**). Amidoxime **22d**: Isolated as an off-white solid. ¹H NMR (500 MHz, DMSO- d_6) δ 8.90 (s, 1H), 7.35 – 7.31 (m, 2H), 7.30 – 7.26 (m, 2H), 5.42 (s, 2H), 3.25 (s, 2H). MS [ESI⁺] m/z : 185.5 [M + H⁺]⁺.

Pyrimidinone ester **26d**: Isolated as a light brown solid. ¹H NMR (500 MHz, DMSO- d_6) δ 12.92 (s, 1H), 10.24 (s, 1H), 7.38 (d, J = 8.5 Hz, 2H), 7.30 (d, J = 8.5 Hz, 2H), 3.81 (s, 2H), 3.79 (s, 3H). MS [ESI⁺] m/z : 295.0 [M + H⁺]⁺.

Inhibitor **9d**: Isolated as a white solid. ¹H NMR (500 MHz, DMSO- d_6) δ 7.40 (d, J = 8.5 Hz, 2H), 7.35 (d, J = 8.5 Hz, 2H), 3.92 (s, 2H). ¹³C NMR (101 MHz, DMSO- d_6) δ 168.0, 159.5, 151.1, 149.5, 135.1, 132.3, 131.1, 129.0, 124.2, 37.8. HRMS [ESI⁻] calculated for C₁₂H₈ClN₂O₄ m/z , 279.01781; found 279.01776 [M - H⁺]⁻.

5.3.1.5. 2-(4-Bromophenyl)-5,6-dihydroxypyrimidine-4-carboxylic acid (**9e**). Amidoxime **22e**: Isolated as off-white solid. ¹H NMR (500 MHz, DMSO- d_6) δ 9.72 (s, 1H), 7.64–7.59 (m, 2H), 7.59–7.55 (m, 2H), 5.85 (br_s, 2H). MS [ESI⁺] m/z : 215.3 [M + H⁺]⁺.

Pyrimidinone ester **22e**: Isolated as a light orange solid. ¹H NMR (400 MHz, DMSO- d_6) δ 7.95 (d, J = 8.7 Hz, 2H), 7.71 (d, J = 8.7 Hz, 2H), 3.85 (s, 3H). MS [ESI⁺] m/z : 325.0 [M + H⁺]⁺.

Inhibitor **9e**: Isolated as off-white solid. ¹H NMR (400 MHz, DMSO- d_6) δ 8.00 (d, J = 8.7 Hz, 2H), 7.71 (d, J = 8.7 Hz, 2H). ¹³C NMR (101 MHz, DMSO- d_6) δ 169.1, 159.5, 149.1, 144.0, 131.5, 131.5, 129.1, 128.3, 124.2. HRMS [ESI⁻] calculated for C₁₁H₆BrN₂O₄ m/z , 308.95164; found 308.95184 [M - H⁺]⁻.

5.3.1.6. 5,6-Dihydroxy-2-(*p*-tolyl)pyrimidine-4-carboxylic acid (**9f**). Amidoxime **22f**: Isolated as a white solid. ¹H NMR (500 MHz, DMSO- d_6) δ 9.51 (s, 1H), 7.56 (d, J = 8.2 Hz, 2H), 7.17 (d, J = 7.9 Hz, 2H), 5.72 (br_s, 2H), 2.31 (s, 3H). MS [ESI⁺] m/z : 151.1 [M + H⁺]⁺.

Pyrimidinone ester **26f**: Isolated as a light orange solid. ¹H NMR (500 MHz, DMSO- d_6) δ 7.91 (d, J = 8.3 Hz, 2H), 7.30 (d, J = 8.0 Hz, 2H), 3.85 (s, 3H), 2.36 (s, 3H). MS [ESI⁺] m/z : 261.1 [M + H⁺]⁺.

Inhibitor **9f**: Isolated as off-white solid. ¹H NMR (400 MHz, DMSO- d_6) δ 7.95 (d, J = 8.3 Hz, 2H), 7.30 (d, J = 8.0 Hz, 2H), 2.36 (s, 3H). ¹³C NMR (101 MHz, DMSO- d_6) δ 169.2, 159.4, 148.2, 145.4, 140.5, 129.4, 129.0, 128.2, 127.1, 20.9. HRMS [ESI⁻] calculated for C₁₂H₉N₂O₄ m/z , 245.05678; found 245.05642 [M - H⁺]⁻.

5.3.1.7. 5,6-Dihydroxy-2-(4-isopropylphenyl)pyrimidine-4-carboxylic acid (**9g**). Amidoxime **22g**: Isolated as a yellow oil that solidified upon standing at rt. ¹H NMR (500 MHz, DMSO- d_6) δ 9.53 (s, 1H), 7.59 (d, J = 8.4 Hz, 2H), 7.24 (d, J = 8.2 Hz, 2H), 5.73 (br_s, 2H), 2.94–2.85 (m, 1H), 1.21 (d, J = 6.9 Hz, 6H). MS [ESI⁺] m/z : 179.1 [M + H⁺]⁺.

Pyrimidinone ester **26g**: Isolated as a very pale orange solid. ¹H NMR (500 MHz, DMSO- d_6) δ 13.02 (br_s, 1H), 10.44 (br_s, 1H), 7.93 (d, J = 8.4 Hz, 2H), 7.37 (d, J = 8.3 Hz, 2H), 3.85 (s, 3H), 3.00–2.90 (m, 1H), 1.22 (d, J = 6.9 Hz, 6H). ¹³C NMR (126 MHz, DMSO- d_6) δ 166.0, 159.5, 151.4, 146.1, 145.0, 129.7, 129.1, 127.2, 126.5, 52.2, 33.3, 23.6. MS [ESI⁺] m/z : 289.1 [M + H⁺]⁺.

Inhibitor **9g**: Isolated as a very pale orange solid. ¹H NMR (400 MHz, DMSO- d_6) δ 7.96 (d, J = 8.3 Hz, 2H), 7.35 (d, J = 8.3 Hz, 2H), 2.94 (hept, J = 6.8 Hz, 1H), 1.22 (d, J = 6.9 Hz, 6H). ¹³C NMR (101 MHz, DMSO- d_6) δ 169.2, 159.4, 151.2, 148.3, 145.3, 129.8, 128.3, 127.2, 126.4, 33.3, 23.6. HRMS [ESI⁻] calculated for C₁₄H₁₃N₂O₄ m/z , 273.08808; found 273.08809 [M - H⁺]⁻.

5.3.1.8. 2-(3-Chlorophenyl)-5,6-dihydroxypyrimidine-4-carboxylic acid (**9h**). Amidoxime **22h**: Isolated as off-white solid. ¹H NMR (500 MHz, DMSO- d_6) δ 9.78 (s, 1H), 7.70 (t, J = 1.7 Hz, 1H), 7.65–7.63

(m, 1H), 7.44–7.38 (m, 2H), 5.89 (br_s, 2H). MS [ESI⁺] m/z : 171.3 [M + H⁺]⁺.

Pyrimidinone ester **26h**: Isolated as a light orange solid. ¹H NMR (500 MHz, DMSO- d_6) δ 13.10 (br_s, 1H), 10.63 (br_s, 1H), 8.06 (t, J = 1.8 Hz, 1H), 8.00–7.95 (m, 1H), 7.60–7.58 (m, 1H), 7.53 (t, J = 7.9 Hz, 1H), 3.86 (s, 3H). MS [ESI⁺] m/z : 281.1 [M + H⁺]⁺.

Inhibitor **9h**: Isolated as off-white solid. ¹H NMR (500 MHz, DMSO- d_6) δ 8.14 (t, J = 1.7 Hz, 1H), 8.02 (d, J = 7.8 Hz, 1H), 7.57 (ddd, J = 7.9, 1.8, 0.9 Hz, 1H), 7.52 (t, J = 7.9 Hz, 1H). ¹³C NMR (126 MHz, DMSO- d_6) δ 169.0, 159.2, 148.5, 144.0, 134.2, 133.4, 130.4, 130.3, 128.1, 127.0, 125.7. HRMS [ESI⁻] calculated for C₁₁H₆ClN₂O₄ m/z , 265.00216; found 265.00224 [M - H⁺]⁻.

5.3.1.9. 2-(3-Bromophenyl)-5,6-dihydroxypyrimidine-4-carboxylic acid (**9i**). Amidoxime **22i**: Isolated as a white solid. ¹H NMR (500 MHz, DMSO- d_6) δ 9.78 (s, 1H), 7.84 (t, J = 1.8 Hz, 1H), 7.70–7.67 (m, 1H), 7.57–7.55 (m, 1H), 7.34 (t, J = 7.9 Hz, 1H), 5.89 (br_s, 2H). MS [ESI⁺] m/z : 215.3 [M + H⁺]⁺.

Pyrimidinone ester **26i**: Isolated as a light orange solid. ¹H NMR (500 MHz, DMSO- d_6) δ 8.20 (t, J = 1.7 Hz, 1H), 8.01 (d, J = 8.0 Hz, 1H), 7.72 (dd, J = 8.0, 1.1 Hz, 1H), 7.47 (t, J = 7.9 Hz, 1H), 3.86 (s, 3H). MS [ESI⁺] m/z : 325.0 [M + H⁺]⁺.

Inhibitor **9i**: Isolated as off-white solid. ¹H NMR (500 MHz, DMSO- d_6) δ 8.28 (t, J = 1.7 Hz, 1H), 8.05 (d, J = 8.0 Hz, 1H), 7.70 (dd, J = 8.0, 1.1 Hz, 1H), 7.45 (t, J = 7.9 Hz, 1H). ¹³C NMR (126 MHz, DMSO- d_6) δ 169.0, 159.3, 148.8, 143.7, 134.4, 133.1, 130.6, 129.8, 128.1, 126.0, 121.8. HRMS [ESI⁻] calculated for C₁₁H₆BrN₂O₄ m/z , 308.95164; found 308.95182 [M - H⁺]⁻.

5.3.1.10. 5,6-Dihydroxy-2-(*m*-tolyl)pyrimidine-4-carboxylic acid (**9j**). Amidoxime **22j**: Isolated as a yellow oil. ¹H NMR (500 MHz, DMSO- d_6) δ 9.55 (s, 1H), 7.49 (s, 1H), 7.45 (d, J = 7.7 Hz, 1H), 7.25 (t, J = 7.6 Hz, 1H), 7.18 (d, J = 7.5 Hz, 1H), 5.73 (s, 2H), 2.32 (s, 3H). MS [ESI⁺] m/z : 151.1 [M + H⁺]⁺.

Pyrimidinone ester **26j**: Isolated as a light orange solid. ¹H NMR (400 MHz, DMSO- d_6) δ 13.00 (s, 1H), 10.50 (s, 1H), 7.84 (s, 1H), 7.79 (d, J = 7.6 Hz, 1H), 7.38 (t, J = 7.6 Hz, 1H), 7.33 (d, J = 7.6 Hz, 1H), 3.85 (s, 3H), 2.37 (s, 3H). ¹³C NMR (126 MHz, DMSO- d_6) δ 166.0, 159.5, 146.2, 145.2, 137.8, 132.0, 131.4, 129.0, 128.5, 127.6, 124.3, 52.3, 20.9. MS [ESI⁺] m/z : 261.1 [M + H⁺]⁺.

Inhibitor **9j**: Isolated as off-white solid. ¹H NMR (500 MHz, DMSO- d_6) δ 7.88 (s, 1H), 7.82 (d, J = 7.7 Hz, 1H), 7.37 (t, J = 7.6 Hz, 1H), 7.32 (d, J = 7.5 Hz, 1H), 2.37 (s, 3H). ¹³C NMR (126 MHz, DMSO- d_6) δ 169.1, 159.2, 147.9, 145.7, 137.8, 132.0, 131.3, 128.4, 128.2, 127.8, 124.3, 20.9. HRMS [ESI⁻] calculated for C₁₂H₉N₂O₄ m/z , 245.05678; found 245.05644 [M - H⁺]⁻.

5.3.1.11. 2-(3-Chloro-4-methylphenyl)-5,6-dihydroxypyrimidine-4-carboxylic acid (**9k**). Amidoxime **22k**: Isolated as a white solid. ¹H NMR (400 MHz, DMSO- d_6) δ 9.68 (s, 1H), 7.67 (d, J = 1.6 Hz, 1H), 7.53 (dd, J = 8.0, 1.7 Hz, 1H), 7.33 (d, J = 8.0 Hz, 1H), 5.84 (br_s, 2H), 2.31 (s, 3H). MS [ESI⁺] m/z : 185.0 [M + H⁺]⁺.

Pyrimidinone ester **26k**: Isolated as a light orange solid. ¹H NMR (500 MHz, DMSO- d_6) δ 8.06 (s, 1H), 7.89 (d, J = 9.1 Hz, 1H), 7.47 (d, J = 8.1 Hz, 1H), 3.86 (s, 3H), 2.38 (s, 3H). ¹³C NMR (126 MHz, DMSO- d_6) δ 165.8, 159.5, 145.6, 144.6, 138.3, 133.6, 131.5, 131.4, 128.8, 127.2, 125.6, 52.3, 19.5. MS [ESI⁺] m/z : 295.0 [M + H⁺]⁺.

Inhibitor **9k**: Isolated as white solid. ¹H NMR (400 MHz, DMSO- d_6) δ 8.13 (d, J = 1.6 Hz, 1H), 7.93 (dd, J = 8.0, 1.7 Hz, 1H), 7.46 (d, J = 8.1 Hz, 1H), 2.38 (s, 3H). ¹³C NMR (101 MHz, DMSO- d_6) δ 169.1, 159.6, 149.7, 143.1, 137.8, 133.5, 131.9, 131.2, 128.1, 127.2, 125.5, 19.5. HRMS [ESI⁻] calculated for C₁₂H₈ClN₂O₄ m/z , 279.01781; found 279.01786 [M - H⁺]⁻.

5.3.1.12. 2-(3-Bromo-4-methylphenyl)-5,6-dihydroxypyrimidine-4-carboxylic acid (**9l**). Amidoxime **22l**: Isolated as a white solid. ¹H

NMR (400 MHz, DMSO- d_6) δ 9.69 (s, 1H), 7.84 (d, J = 1.7 Hz, 1H), 7.57 (dd, J = 7.9, 1.7 Hz, 1H), 7.33 (d, J = 8.0 Hz, 1H), 5.86 (br_s, 2H), 2.32 (s, 3H). MS [ESI⁺] m/z : 228.99 [M + H⁺]⁺.

Pyrimidinone ester 26l: Isolated as light orange solid. ¹H NMR (500 MHz, DMSO- d_6) δ 8.23 (d, J = 1.7 Hz, 1H), 7.93 (dd, J = 8.0, 1.8 Hz, 1H), 7.47 (d, J = 8.1 Hz, 1H), 3.86 (s, 3H), 2.39 (s, 3H). ¹³C NMR (126 MHz, DMSO- d_6) δ 165.8, 159.5, 145.5, 144.5, 140.1, 131.6, 131.1, 130.4, 128.8, 126.2, 124.3, 52.3, 22.3. HRMS [ESI⁻] calculated for C₁₃H₁₀BrN₂O₄ m/z , 336.9829; found 336.9834 [M – H⁺]⁻.

Inhibitor 9l: Isolated as white solid. ¹H NMR (400 MHz, DMSO- d_6) δ 8.31 (d, J = 1.7 Hz, 1H), 7.97 (dd, J = 8.0, 1.8 Hz, 1H), 7.46 (d, J = 8.2 Hz, 1H), 2.39 (s, 3H). ¹³C NMR (101 MHz, DMSO- d_6) δ 169.0, 159.3, 148.5, 143.8, 139.9, 131.7, 131.1, 130.5, 128.1, 126.2, 124.3, 22.3. HRMS [ESI⁺] calculated for C₁₂H₁₀BrN₂O₄ m/z , 324.9818 found 324.9820 [M + H⁺]⁺.

5.3.1.13. **2-(4-(3,5-Dimethylisoxazol-4-yl)phenyl)-5,6-dihydroxypyrimidine-4-carboxylic acid (9m)**. The nitrile, 4-(3,5-dimethylisoxazol-4-yl)benzotrile²⁸ was prepared via Suzuki cross-coupling between (3,5-dimethylisoxazol-4-yl)boronic acid and 4-bromobenzotrile.

Amidoxime 22m: Isolated as a white solid and used directly in the next step.

Pyrimidinone ester 26m: Isolated as orange solid. ¹H NMR (400 MHz, DMSO- d_6) δ 8.11 (d, J = 8.3 Hz, 2H), 7.53 (d, J = 8.3 Hz, 2H), 3.86 (s, 3H), 2.44 (s, 3H), 2.26 (s, 3H).

Inhibitor 9m: Isolated as a white solid. ¹H NMR (400 MHz, DMSO- d_6) δ 8.13 (d, J = 8.3 Hz, 2H), 7.51 (d, J = 8.3 Hz, 2H), 2.44 (s, 3H), 2.26 (s, 3H). HRMS [ESI⁻] calculated for C₁₆H₁₂N₃O₅ m/z , 326.0782; found 326.0783 [M – H⁺]⁻.

5.3.1.14. **2-(3',4'-Difluoro-[1,1'-biphenyl]-3-yl)-5,6-dihydroxypyrimidine-4-carboxylic acid (9n)**. The nitrile, 3',4'-difluoro-[1,1'-biphenyl]-3-carbonitrile was prepared from 3-bromobenzotrile and 3,4-difluorophenyl boronic acid as Suzuki cross-coupling partners. ¹H NMR (400 MHz, CDCl₃) δ 7.80 (s, 1H), 7.75 (d, J = 7.9 Hz, 1H), 7.66 (d, J = 7.7 Hz, 1H), 7.56 (t, J = 7.8 Hz, 1H), 7.41 – 7.32 (m, 1H), 7.29–7.27 (m, 2H). MS [ESI⁺] m/z : 216.1 [M + H⁺]⁺.

Amidoxime 22n: Isolated as off-white solid and used directly in the next step.

Pyrimidinone ester 26n: Isolated as a light orange solid. ¹H NMR (400 MHz, DMSO- d_6) δ 8.29 (s, 1H), 8.04 (d, J = 8.0 Hz, 1H), 7.96–7.94 (m, 1H), 7.86 (d, J = 7.6 Hz, 1H), 7.69–7.67 (m, 1H), 7.63 – 7.57 (m, 2H), 3.86 (s, 3H). MS [ESI⁺] m/z : 359.1 [M + H⁺]⁺.

Inhibitor 9n: Isolated as a white solid. ¹H NMR (500 MHz, DMSO- d_6) δ 8.31 (s, 1H), 8.09 (d, J = 7.9 Hz, 1H), 7.97–7.92 (m, 1H), 7.83 (d, J = 8.0 Hz, 1H), 7.70–7.68 (m, 1H), 7.61–7.56 (m, 2H). HRMS [ESI⁻] calculated for C₁₇H₉F₂N₂O₄ m/z , 343.0536; found 343.0531 [M – H⁺]⁻.

5.3.1.15. **2-(3,5-Bis(trifluoromethyl)phenyl)-5,6-dihydroxypyrimidine-4-carboxylic acid (9o)**. **Amidoxime 22o**: Isolated as off-white solid. ¹H NMR (500 MHz, DMSO- d_6) δ 10.10 (s, 1H), 8.32 (s, 2H), 6.22 (br_s, 2H). MS [ESI⁺] m/z : 273.0 [M + H⁺]⁺.

Pyrimidinone ester 26o: Isolated as a light yellow solid. ¹H NMR (400 MHz, DMSO- d_6) δ 8.66 (s, 2H), 8.27 (s, 1H), 3.86 (s, 3H). MS [ESI⁺] m/z : 383.0 [M + H⁺]⁺.

Inhibitor 9o: Isolated as a white solid. ¹H NMR (500 MHz, DMSO- d_6) δ 8.77 (s, 2H), 8.26 (s, 1H). ¹³C NMR (101 MHz, DMSO- d_6) δ 169.2, 159.8, 150.0, 143.0, 135.3, 131.1 (q, J = 33.2 Hz), 128.2 (br), 124.1 (br), 123.7 (q, J = 273.0 Hz). HRMS [ESI⁻] calculated for C₁₃H₅F₆N₂O₄ m/z , 367.0159; found 367.0143 [M – H⁺]⁻.

5.4. Synthesis of Adenine-based compounds 9p and 9q

The corresponding adenine-containing nitriles were prepared based on literature procedures with slight modifications.²¹

Step 1: The amidoxime intermediates **29a–b** were prepared using the protocol described for **22**.

Step 2: Michael adducts **30a–b** were prepared as follows: to the solution of amidoxime **29** (1.0 eq) in DMSO (3.0 mL per 1.0 mmol **29**) was added Et₃N (0.1–1.0 eq; Note: 0.1 eq was used for **29b** and up to 1.0 eq for **29a**). DMAD (1.1 eq) was then added dropwise to the resulting mixture. Reaction was stirred at rt for ~4–16 h (monitored by LC-MS). The mixture was diluted with H₂O and then extracted with EtOAc. The organic layer was collected and the aqueous layer was further extracted with EtOAc/*n*-butanol (1:1). The organic layers were combined, washed with semi-brine then dried *in vacuo*. Crude product was purified by silica gel chromatography (gradient of 50% EtOAc in hexanes to 100% EtOAc, then to 20% MeOH in EtOAc). Michael adduct **30** was isolated as dark brown oil in ~50% yield (for **30a**, based on recovered starting material) to ~80% yield (for **30b**) and was used immediately in the next step.

Step 3: Preparation of pyrimidinone ester **32a–b** Michael adduct **30** (1.0 eq) and CuBr (50 mol%)²⁰ were weighed in an oven-dried vial. Air was removed by vacuum and the vial was purged with Ar. Dry dioxane (1.0 mL per 0.1 mmol **30**) was added and the vial was evacuated again and purged with Ar. The mixture was sonicated for ~30 s and then stirred at 130 °C for 30 min under Ar. The reaction mixture was cooled to rt and then diluted with 1:1 MeOH:H₂O. CuBr was removed *via* filtration. The filtrate was collected, concentrated, and the remaining H₂O was removed using a lyophilizer. Crude product (**32**) was purified by reversed phase chromatography; isolated yield was ~30%.

Step 4: Ester hydrolysis to give **9p** and **9q** was done the same way as described for **9a–9o**; final compounds were purified by trituration.

5.4.1. 2-((6-Amino-9H-purin-9-yl)methyl)-5,6-dihydroxypyrimidine-4-carboxylic acid (9p)

5.4.1.1. **Amidoxime 29a**. Isolated as a light yellow solid. ¹H NMR (400 MHz, DMSO- d_6) δ 9.26 (s, –OH), 8.15 (s, 1H), 8.11 (s, 1H), 7.21 (br_s, –NH₂), 5.68 (s, –NH₂), 4.75 (s, 2H). ¹³C NMR (126 MHz, DMSO- d_6) δ 156.4, 152.9, 150.2, 148.9, 141.7, 118.9, 43.2. MS [ESI⁺] m/z : 208.15 [M + H⁺]⁺.

5.4.2. Michael adduct 30a

Isolated as a dark brown oil. ¹H NMR (400 MHz, DMSO- d_6) δ 8.14 (s, 1H), 8.12 (s, 1H), 7.24 (br_s, 2H), 6.91 (br_s, 2H), 5.41 (s, 1H), 4.91 (s, 2H), 3.70 (s, 3H), 3.56 (s, 3H). MS [ESI⁺] m/z : 350.1 [M + H⁺]⁺.

5.4.3. Pyrimidinone ester 32a

Isolated as brown solid. ¹H NMR (400 MHz, DMSO- d_6) δ 8.16 (s, 1H), 8.12 (s, 1H), 7.24 (br_s, 2H), 5.23 (s, 2H), 3.74 (s, 3H). MS [ESI⁺] m/z : 318.0 [M + H⁺]⁺.

5.4.4. Inhibitor 9p

Isolated as a light yellow solid. ¹H NMR (400 MHz, D₂O added with 1.5–2.0 eq NaOH) δ 8.24 (s, 1H), 8.22 (s, 1H), 5.25 (s, 2H). ¹³C NMR (101 MHz, D₂O added with 1.5–2.0 eq NaOH) δ 173.8, 168.9, 155.4, 152.9, 152.4, 149.1, 146.0, 142.9, 133.6, 118.3, 48.9. HRMS [ESI⁻] calculated for C₁₁H₈N₇O₄ m/z , 302.06433; found 302.06431 [M – H⁺]⁻.

5.4.5. 2-(2-(6-Amino-9H-purin-9-yl)ethyl)-5,6-dihydroxypyrimidine-4-carboxylic acid (9q)

Amidoxime 29b: Isolated as a white solid. ¹H NMR (500 MHz, DMSO- d_6) δ 8.91 (s, –OH), 8.14 (s, 1H), 8.01 (s, 1H), 7.16

(br_s, —NH₂), 5.51 (s, —NH₂), 4.33 (t, *J* = 7.1 Hz, 2H), 2.54 (t, *J* = 7.1 Hz, 2H). ¹³C NMR (126 MHz, DMSO-d₆) δ 156.4, 152.8, 150.2, 149.9, 141.3, 119.2, 40.4, 31.6. HSQC (¹H–¹³C): ¹H δ 4.33 correlates to ¹³C δ 40.4. MS [ESI⁺] *m/z*: 222.10 [M + H]⁺.

Michael adduct 30b: Isolated as a brown oil. ¹H NMR (500 MHz, DMSO-d₆) δ 8.14 (s, 1H), 8.04 (s, 1H), 7.16 (br_s, 2H), 6.68 (br_s, 2H), 5.50 (s, 1H), 4.37 (t, *J* = 7.0 Hz, 2H), 3.74 (s, 3H), 3.58 (s, 3H), 2.70 (t, *J* = 7.0 Hz, 2H). MS [ESI⁺] *m/z*: 364.1 [M + H]⁺.

Pyrimidinone ester 32b: Isolated as a brown solid. ¹H NMR (400 MHz, DMSO-d₆) δ 8.13 (s, 1H), 8.12 (s, 1H), 7.15 (br_s, 2H), 4.48 (t, *J* = 6.7 Hz, 2H), 3.78 (s, 3H), 2.98 (t, *J* = 6.7 Hz, 2H). MS [ESI⁺] *m/z*: 332.1 [M + H]⁺.

Inhibitor 9q: Isolated as a beige solid. ¹H NMR (500 MHz, DMSO-d₆ with ~2% ND₄OD) δ 8.21 (s, 1H), 8.13 (s, 1H), 7.14 (br_s, 2H), 4.48 (br, 2H), 2.92 (br, 2H). HRMS [ESI⁻] calculated for C₁₂H₁₀N₇O₄ *m/z*, 316.07998; found 316.08006 [M – H]⁻.

5.5. General protocol for the synthesis of Pyridopyrimidine-based compounds 9r–9v

Step 1: Preparation of **39i–iv** Amine **38b** (1.1–1.3 eq) and Et₃N (3.0 eq) were dissolved in dry DMSO (~2.0 mL per 0.15 mmol **38b**) and stirred at rt for 5 min. The aryl chloride **37** (1.0 eq; dissolved in 1.0 mL dry dioxane) was then added and the mixture was heated at 100 °C for 1 h (under Ar balloon). The reaction was cooled to rt, concentrated *in vacuo*, added with H₂O (to crash out the product), and then filtered. Crude product **39** was purified by trituration. Typical isolated yield was ~50–70%. When R₆ of **39** was bromide, Suzuki cross-coupling was used to introduce several aryl groups at the R₆ position, as previously described²⁹; product was purified by trituration.

Step 2: Ester hydrolysis of **39** to give the pyridopyrimidine-based compounds **9r–9v** was done as described for **9a–9o**. Final compounds were converted first to their corresponding monosodium salt prior to purification by reversed-phase prep chromatography.

5.5.1. 5,6-Dihydroxy-2-((pyrido[2,3-d]pyrimidin-4-ylamino)methyl)pyrimidine-4-carboxylic acid (9r)

Pyrimidinone ester 39i: Isolated as a reddish-brown solid. ¹H NMR (400 MHz, DMSO-d₆) δ 12.87 (br_s, 1H), 10.26 (br_s, 1H), 9.09 (br, —NH), 9.02 (d, *J* = 4.2 Hz, 1H), 8.73 (d, *J* = 7.4 Hz, 1H), 8.60 (s, 1H), 7.60 (dd, *J* = 8.1, 4.3 Hz, 1H), 4.57 (d, *J* = 4.7 Hz, 2H), 3.76 (s, 3H). MS [ESI⁺] *m/z*: 329.1 [M + H]⁺.

Final inhibitor 9r: Isolated as a light orange solid. ¹H NMR (500 MHz, DMSO-d₆ with ~2% ND₄OD) δ 8.99 (dd, *J* = 4.3, 1.8 Hz, 1H), 8.76 (dd, *J* = 8.2, 1.6 Hz, 1H), 8.59 (s, 1H), 7.56 (dd, *J* = 8.2, 4.4 Hz, 1H), 4.53 (s, 2H). ¹³C NMR (101 MHz, DMSO-d₆ with ~2% ND₄OD) δ 169.0, 162.2, 160.8, 158.1, 158.1, 155.8, 151.6, 144.5, 133.0, 127.6, 121.5, 109.9, 43.0. HRMS [ESI⁻] calculated for C₁₃H₉N₆O₄ *m/z*, 313.06908; found 313.06909 [M – H]⁻.

5.5.2. 2-(((6-Bromopyrido[2,3-d]pyrimidin-4-yl)amino)methyl)-5,6-dihydroxypyrimidine-4-carboxylic acid (9s)

Pyrimidinone ester 39ii: Isolated as a brown solid. ¹H NMR (500 MHz, DMSO-d₆) δ 9.17 (br, —NH), 9.10 (d, *J* = 2.2 Hz, 1H), 9.07 (br, 1H), 8.64 (s, 1H), 4.58 (d, *J* = 5.1 Hz, 2H), 3.78 (s, 3H). MS [ESI⁺] *m/z*: 407.0 [M + H]⁺.

Inhibitor 9s: Isolated as a yellow solid. ¹H NMR (500 MHz, DMSO-d₆ with ~2% ND₄OD) δ 9.13 (d, *J* = 2.3 Hz, 1H), 9.10 (d, *J* = 2.3 Hz, 1H), 8.70 (s, 1H), 4.65 (s, 2H). ¹³C NMR (126 MHz, DMSO-d₆ with ~2% ND₄OD) δ 171.0, 164.4, 160.3, 158.8, 156.6, 156.5, 149.6, 148.4, 135.7, 130.7, 115.9, 111.2, 44.7. HRMS [ESI⁻] calculated for C₁₃H₈BrN₆O₄ *m/z*, 390.9796; found 390.9801 [M – H]⁻.

5.5.3. 2-(((6-Bromo-7-(methylthio)pyrido[2,3-d]pyrimidin-4-yl)amino)methyl)-5,6-dihydroxypyrimidine-4-carboxylic acid (9t)

Pyrimidinone ester 39iii: Isolated as a brown solid. ¹H NMR (400 MHz, DMSO-d₆) δ 9.02 (br, —NH), 8.91 (s, 1H), 8.56 (s, 1H), 4.53 (br, 2H), 3.76 (s, 3H), 2.61 (s, 3H). MS [ESI⁺] *m/z*: 453.0 [M + H]⁺.

Inhibitor 9t: Isolated as a light orange solid. ¹H NMR (500 MHz, DMSO-d₆ with ~2% ND₄OD) δ 8.94 (s, 1H), 8.64 (s, 1H), 4.62 (s, 2H), 2.63 (s, 3H). ¹³C NMR (126 MHz, DMSO-d₆ with ~2% ND₄OD) δ 171.4, 166.9, 165.4, 159.9, 158.8, 156.7, 149.7, 149.0, 135.3, 131.1, 114.6, 107.5, 45.0, 14.5. HRMS [ESI⁻] calculated for C₁₄H₁₀-BrN₆O₄S *m/z*, 436.9673; found 436.9668 [M – H]⁻.

5.5.4. 5,6-Dihydroxy-2-(((6-(4-methoxyphenyl)pyrido[2,3-d]pyrimidin-4-yl)amino)methyl)pyrimidine-4-carboxylic acid (9u)

Pyrimidinone ester 39iv: Prepared via Suzuki cross-coupling between **39ii** and 4-methoxyphenyl boronic acid. Isolated as a brown solid. ¹H NMR (400 MHz, DMSO-d₆) δ 9.36 (s, 1H), 9.14 (br_s, —NH), 9.00 (s, 1H), 8.58 (s, 1H), 7.85 (d, *J* = 8.2 Hz, 2H), 7.14 (d, *J* = 8.5 Hz, 2H), 4.60 (d, *J* = 4.2 Hz, 2H), 3.84 (s, 3H), 3.77 (s, 3H). MS [ESI⁺] *m/z*: 435.1 [M + H]⁺.

Inhibitor 9u: Isolated as a light yellow solid. ¹H NMR (500 MHz, DMSO-d₆ with ~2% ND₄OD) δ 9.31 (d, *J* = 2.5 Hz, 1H), 9.00 (d, *J* = 2.3 Hz, 1H), 8.55 (s, 1H), 7.83 (d, *J* = 8.6 Hz, 2H), 7.11 (d, *J* = 8.6 Hz, 2H), 4.56 (s, 2H), 3.83 (s, 3H). ¹³C NMR (101 MHz, DMSO-d₆ with ~2% ND₄OD) δ 169.6, 162.5, 160.9, 159.7, 157.6, 156.8, 153.8, 151.2, 145.7, 132.6, 129.0, 128.6, 128.5, 128.4, 114.8, 109.7, 55.5, 43.5. HRMS [ESI⁻] calculated for C₂₀H₁₅N₆O₅ *m/z*, 419.1109; found 419.1115 [M – H]⁻.

5.5.5. 5,6-Dihydroxy-2-(((6-(4-methoxyphenyl)-7-(methylthio)pyrido[2,3-d]pyrimidin-4-yl)amino)methyl)pyrimidine-4-carboxylic acid (9v)

Pyrimidinone ester 39v: Prepared via Suzuki cross-coupling between **39iii** and 4-methoxyphenyl boronic acid. Product was isolated as a brown solid. ¹H NMR (500 MHz, DMSO-d₆) δ 8.70 (br_s, —NH), 8.53 (s, 1H), 8.39 (s, 1H), 7.46 (d, *J* = 8.6 Hz, 2H), 7.07 (d, *J* = 8.6 Hz, 2H), 4.37 (d, *J* = 4.7 Hz, 2H), 3.82 (s, 3H), 3.60 (s, 3H), 2.54 (s, 3H). MS [ESI⁺] *m/z*: 481.1 [M + H]⁺.

Inhibitor 9v: Isolated as a slightly brown solid. ¹H NMR (500 MHz, DMSO-d₆ with ~2% ND₄OD) δ 8.72 (s, 1H), 8.49 (s, 1H), 7.47 (d, *J* = 8.5 Hz, 2H), 7.10 (d, *J* = 8.6 Hz, 2H), 4.65 (s, 2H), 3.84 (s, 3H), 2.58 (s, 3H). HRMS [ESI⁻] calculated for C₂₁H₁₇N₆O₅S *m/z*, 465.0987; found 465.0984 [M – H]⁻.

5.6. 2-(3-Bromo-4-methylphenyl)-5,6-dihydroxy-N-methylpyrimidine-4-carboxamide (27I)

Prepared based on previously described protocols^{2,30} using **26I** and methylamine (33 wt% in EtOH) as starting materials. Isolated as off-white solid (~80% yield). ¹H NMR (500 MHz, DMSO-d₆) δ 12.89 (br_s, 1H), 12.84 (br_s, 1H), 9.08 (br_s, 1H), 8.51 (d, *J* = 1.6 Hz, 1H), 8.16 (d, *J* = 6.9 Hz, 1H), 7.48 (d, *J* = 8.2 Hz, 1H), 2.87 (d, *J* = 4.9 Hz, 3H), 2.41 (s, 3H). ¹³C NMR (101 MHz, DMSO-d₆) δ 168.9, 158.4, 148.0, 144.4, 140.3, 131.2, 130.9, 130.7, 126.9, 126.5, 124.5, 25.8, 22.4. HRMS [ESI⁺] calculated for C₁₃H₁₃BrN₃O₃ *m/z*, 338.0135 found 338.0140 [M + H]⁺.

5.7. Pyrido[2,3-d]pyrimidin-4(3H)-one (36i)

Prepared via reaction of 2-aminonicotinic acid (1.0 eq) with formamide (50.0 eq) at 145 °C for 20 h.³¹ Isolated as a beige solid (1.6 g, 58%). ¹H NMR (500 MHz, DMSO-d₆) δ 12.55 (br_s, 1H), 8.95 (dd, *J* = 4.5, 2.0 Hz, 1H), 8.51 (dd, *J* = 7.9, 2.0 Hz, 1H), 8.32 (s, 1H), 7.55 (dd, *J* = 7.9, 4.6 Hz, 1H). ¹³C NMR (126 MHz, DMSO-d₆) δ 162.1, 159.1, 156.2, 149.2, 136.1, 123.0, 118.3. MS [ESI⁺] *m/z*: 148.0 [M + H]⁺.

5.8. 6-Bromopyrido[2,3-d]pyrimidin-4(3H)-one (**36ii**)

Prepared in two ways, however, both provide equivalent isolated yields: (a) Reaction of 2-amino-5-bromonicotinic acid (1.0 eq) with formamide (50.0 eq) at 145 °C for 20 h (68%, isolated as beige solid),³¹ or (b) by treating of 6-bromopyrido[2,3-d]pyrimidin-4-amine⁵ with methane sulfonic acid/H₂O at 100 °C (60%)³¹. ¹H NMR (500 MHz, DMSO-d₆) δ 12.74 (br_s, 1H), 9.05 (d, *J* = 2.6 Hz, 1H), 8.63 (d, *J* = 2.6 Hz, 1H), 8.36 (s, 1H).

5.9. 6-Bromo-7-(methylthio)pyrido[2,3-d]pyrimidin-4(3H)-one (**36iii**)

Prepared by treatment of 6-bromo-7-(methylthio)pyrido[2,3-d]pyrimidin-4-amine⁵ with methane sulfonic acid/H₂O³² at 100 °C. Isolated as a yellow solid. ¹H NMR (400 MHz, DMSO-d₆) δ 12.65 (br_s, 1H), 8.44 (s, 1H), 8.32 (s, 1H), 2.61 (s, 3H). ¹³C NMR (126 MHz, DMSO-d₆) δ 166.4, 160.9, 157.8, 150.0, 137.3, 116.1, 115.5, 14.9.

5.10. General protocol for the synthesis of **37i–iii**

Chlorination was carried out using a literature protocol with minor modifications.³³ In summary, pyridopyrimidinone **36** (1.0 eq), dry toluene (~1.0 mL per 1.0 mmol **36**), and pyridine (1.0 eq) were mixed in the pressure vessel. POCl₃ (5.0 eq) was added with stirring. The tube was then sealed and heated at 115 °C (in the case of **36iii**) or at 180 °C (in the case of **36i–ii**) for ~2 h. The reaction was cooled, concentrated *in vacuo*, diluted with EtOAc, and washed with cold NaHCO₃ solution, dried over Na₂SO₄ and concentrated *in vacuo*. The crude product was purified by silica gel chromatography (24 g column, 2%–85% EtOAc in hexanes with 0.1% Et₃N) and used immediately in the next step. Isolated yields were typically ~30–65%.

5.10.1. 4-Chloropyrido[2,3-d]pyrimidine (**37i**)

Isolated as a light yellow solid. ¹H NMR (500 MHz, CDCl₃) δ 9.33 (dd, *J* = 4.3, 1.9 Hz, 1H), 9.27 (s, 1H), 8.65 (dd, *J* = 8.3, 1.9 Hz, 1H), 7.72 (dd, *J* = 8.3, 4.3 Hz, 1H). ¹³C NMR (126 MHz, CDCl₃) δ 163.3, 158.8, 158.8, 157.1, 135.3, 124.6, 119.5. MS [ESI⁺] *m/z*: 166.0 [M + H⁺]⁺.

5.10.2. 6-Bromo-4-chloropyrido[2,3-d]pyrimidine (**37ii**)

Isolated as a light yellow solid. ¹H NMR (400 MHz, CDCl₃) δ 9.32 (d, *J* = 2.5 Hz, 1H), 9.30 (s, 1H), 8.78 (d, *J* = 2.5 Hz, 1H).

5.10.3. 6-Bromo-4-chloro-7-(methylthio)pyrido[2,3-d]pyrimidine (**37iii**)

Isolated as a yellow solid. ¹H NMR (500 MHz, CDCl₃) δ 9.15 (s, 1H), 8.53 (s, 1H), 2.77 (s, 3H). ¹³C NMR (126 MHz, CDCl₃) δ 172.2, 161.3, 157.4, 157.1, 135.2, 120.3, 117.4, 15.6.

5.11. Methyl 2-(aminomethyl)-5,6-dihydroxypyrimidine-4-carboxylate (**38b**)

Step 1: Intermediate **38a** was prepared starting from *N*-(Benzyloxycarbonyl)-2-aminoacetonitrile following the sequence of steps described for the synthesis of analogs of **26**. The product was isolated as a beige solid. ¹H NMR (400 MHz, DMSO-d₆) δ 12.73 (s, 1H), 10.32 (s, 1H), 7.65 (t, *J* = 5.8 Hz, 1H), 7.41 – 7.22 (m, 5H), 5.05 (s, 2H), 4.05 (d, *J* = 5.9 Hz, 2H), 3.81 (s, 3H). MS [ESI⁺] *m/z*: 334.1 [M + H⁺]⁺.

Step 2: A mixture of **38a** (1.0 g, 3.0 mmol) was treated with 6 N HCl (0.50 mL; 3.0 mmol), and 10% Pd/C (200 mg) in MeOH (60.0 mL). Once conversion of all starting material was observed by TLC, the reaction mixture was filtered through Celite, then washed with additional MeOH (~50 mL). The combined filtrate was concentrated

and dried under vacuum to afford product as its HCl salt (light orange solid; 540.0 mg, 76%). ¹H NMR (500 MHz, DMSO-d₆) δ 13.26 (br_s, 1H), 10.53 (br_s, 1H), 8.55 (br_s, 3H (–NH₂·HCl)), 3.95 (s, 2H), 3.83 (s, 3H). ¹³C NMR (126 MHz, DMSO-d₆) δ 165.9, 158.9, 146.0, 144.4, 128.8, 52.7, 39.6. –CH₂NH₂ was observed by HSQC (¹H–¹³C): ¹H δ 3.95 correlates to ¹³C δ 39.6. MS [ESI⁺] *m/z*: 200.1 [M + H⁺]⁺.

5.12. Enzymes and nucleic acids

Heterodimeric, HIV-1 RT (p66/p51) was expressed and purified as described previously.³⁴ All nucleic acids were synthesized through IDT DNA Technologies. The following sequences were used:

PPT24: 5'-CCACTTTTTAAAAGAAAAGGGGGG-3'

8a: 5'-TTCTGACTAAAAGGTCTGAGGGAT-3'

PPT57: 5'-CGTTGGGAGTGAATTAGCCCTCCAGTCCCCCTTTTCTTTAAAAA-GTGGCTAAGA-3'

PBS36c: 5'-GTAAGTACTAGATCCCTCAGACCCTTTTAGTCAGAAT-3'

PBS-22dpol: 5'-CTAGCAGTGGCGCCGGAACAGG-3'

PBS-14r8d: 5'-cuguucggcgccaCTGCTAGA-3'

5'-radiolabeling was performed with [γ-³²P]ATP (PerkinElmer Life Sciences) and T4 polynucleotide kinase (Fermentas). Reactions occurred for 1 h at 37 °C. Labeled RNA was subjected to phenol-chloroform emulsification and purified further with P-30 size exclusion columns (Bio-Rad). 5' fluorescent labelling was applied to terminal amino-modified sequences. Briefly, amino modified sequences (roughly 20 nmol) were exposed to 5x excess Cy5 dye in 80 mM sodium bicarbonate and allowed to vortex vigorously overnight. Labeled sequences were separated on a 12% denaturing acrylamide gel, extracted and then purified through ethanol precipitation.

5.13. DNA synthesis assay

A 3-fold molar excess of PPT57 DNA template was heat-annealed to 50 nM 5'-Cy5-labeled PPT24 primer. Substrate was then incubated with 200 nM of RT in a buffer containing 50 mM Tris-HCl pH 7.8, 50 mM NaCl and 6 mM MgCl₂. Inhibitors were titrated up to 250 μM (permitting only a maximum 5% final DMSO concentration where applicable) and were added to the samples which were then pre-incubated at 37 °C for 10 min before starting the reaction. The reaction was initiated with 0.5 μM of each of dATP, dTTP, dGTP, and dCTP and allowed to proceed for 5 min. The reaction was stopped with 100% formamide loading dye containing traces of bromophenol blue. As a negative control, a lane lacking dNTP was used. Samples were loaded on a 12% denaturing polyacrylamide gel and resolved by phosphorimaging (AmershamBiosciences). Inhibitory pausing sites were quantified through QuantityOne software. Percent inhibition was calculated as total inhibitory product divided by full-length product plus inhibitory products multiplied by 100. The product fractions were normalized and plotted against inhibitor concentration using GraphPad Prism software; the normalized data was fitted to a log [Inhibitor] versus response curve with variable slope to extract IC₅₀ values for the inhibition of RT enzyme.

5.14. Site-specific foot-printing assay

Chemical footprinting with Fe²⁺ was performed using 50 nM 5'-radiolabeled DNA template (PBS36c) annealed to 150 nM of the primer (8a). The hybrid was incubated with 750 nM HIV-1 RT in a buffer containing 120 mM sodium cacodylate (pH 7), 20 mM NaCl, and 6 mM MgCl₂ in a final volume of 20 μL. Fixed or increasing concentrations of compound were then added to the samples, followed by pre-incubation of complexes at 37 °C for 10 min prior

to the addition of Fe²⁺. Treatment with Fe²⁺ was conducted using the same method as previously described [16b,17].

5.15. HIV-1 RT, RNase H assay

A 3-fold molar excess PBS-22dpol was heat annealed to 50 nM of 5'-radiolabeled PBS-14r8d. 250 nM HIV-1 RT was incubated in a buffer of 50 mM Tris-HCl (pH 7.8), 50 mM NaCl, 0.2 mM EDTA, 6 mM MgCl₂. Inhibitors were titrated up to 250 μM (permitting only a maximum 5% final DMSO concentration, where applicable) and were added to the samples which were then pre-incubated at 37 °C for 10 min before starting the reaction. The reaction was initiated by the addition of 50 nM preformed DNA-RNA/DNA hybrid and allowed to proceed for 5 min. As positive and negative controls, β-thujaplicinol, a known RNase H inhibitor, and a lane lacking MgCl₂, respectively, were used. Bands were quantified by QuantityOne software (Bio-Rad) and results were graphed using GraphPad Prism. Briefly, % inhibition was calculated by dividing primary cleavage over total cleavage and multiplying by 100, thus, IC₅₀ values are reported as values inhibiting secondary cleavage.

Acknowledgment

Financial support for this work was provided by the Canadian Institute of Health Research (CIHR) to M. Götte and Y.S. Tsantrizos.

A. Supplementary data

Supplementary data associated with this article can be found, in the online version, at <https://doi.org/10.1016/j.bmc.2018.02.017>.

References

- (a) Summa V, Petrocchi A, Pace P, et al. *J Med Chem.* 2004;47:14–17;
(b) Summa V, Petrocchi A, Matassa VG, et al. *J Med Chem.* 2004;47:5336–5339.
- (a) Summa V, Petrocchi A, Matassa VG, et al. *J Med Chem.* 2006;49:6646–6649;
(b) Summa V, Petrocchi A, Bonelli F, et al. *J Med Chem.* 2008;51:5843–5855.
- Johns, BA.; Kawasuji, T.; Taishi, T.; Taoda, Y. US 2009/0318421 A1.
- Di Santo R. *J Med Chem.* 2014;57:539–566.
- Lacbay CM, Mancuso J, Lin Y-S, Bennett N, Götte M, Tsantrizos YS. *J Med Chem.* 2014;57:7435–7449.
- (a) Marchand B, Götte M. *J Biol. Chem.* 2003;278:35362–35372;
(b) Marchand B, Tchesnokov EP, Götte M. *J Biol. Chem.* 2007;282:3337–3346;
(c) Das K, Balzarini J, Miller MT, Maguire AR, DeStefano JJ, Arnold E. *ACS Chem Biol.* 2016;11:2158–2164.
- Freisz S, Bec G, Radi M, et al. *Angew Chem Int Ed.* 2010;49:1805–1808.
- (a) Tang J, Liu F, Nagy E, et al. *J Med Chem.* 2016;59:2648–2659;
(b) Kankanala J, Kirby KA, Liu F, et al. *J Med Chem.* 2016;59:5051–5062;
(c) Vernekar SKV, Liu Z, Nagy E, et al. *J Med Chem.* 2015;58:651–664;
(d) Williams PD, Staas DD, Venkatraman S, et al. *Bioorg. Med. Chem. Lett.* 2010;20:6754–6757.
- Kirschberg TA, Balakrishnan M, Squires NH, et al. *J Med Chem.* 2009;52:5781–5784.
- Stansfield I, Avolio S, Colarusso S, et al. *Bioorg. Med. Chem. Lett.* 2004;14:5085–5088.
- Koch U, Attenni B, Malancona S, et al. *J Med Chem.* 2006;49:1693–1705.
- Cowan JA. *Chem. Rev.* 1998;98:1067–1088.
- Rogolino D, Carcelli M, Sechi M, Neamati N. *Coord. Chem. Rev.* 2012;256:3063–3086.
- Bernatchez JA, Paul R, Tchesnokov EP, et al. *J Biol. Chem.* 2015;290:1474–1484.
- (a) Balzarini J, Das K, Bernatchez JA, et al. *Proc. Natl. Acad. Sci.* 2015;112:3475–3480;
(b) Keane SJ, Ford A, Mullins ND, et al. *J. Org. Chem.* 2015;80:2479–2493.
- Jochmans D, Deval J, Kesteleyn B, et al. *J. Virol.* 2006;80:12283–12292.
- Rajotte D, Tremblay S, Pelletier A, et al. *Antimicrob. Agents Chemother.* 2013;57:2712–2718.
- (a) Dreher SD, Ikemoto N, Gresham V, et al. *D. Tetrahedron Lett.* 2004;45:6023–6025;
(b) Humphrey GR, Pye PJ, Zhong Y-L, et al. *Org. Process Res. Dev.* 2011;15:73–83;
(c) Zhong Y-L, Zhou H, Gauthier Jr DR, Askin D. *Tetrahedron Lett.* 2006;47:1315–1317.
- Pye PJ, Zhong Y-L, Jones GO, Reamer RA, Houk KN, Askin D. *Angew. Chem. Int. Ed.* 2008;47:4134–4136.
- Bellomo A, Celebi-Olcum N, Bu X, et al. *Angew. Chem. Int. Ed.* 2012;51:6912–6915.
- (a) Hocková D, Buděšínský M, Marek R, Marek J, Holý A. *Eur. J. Org. Chem.* 1999;2675–2682;
(b) Hakimelahi GH, Ly TW, Moosavi-Movahedi AA, et al. *J Med Chem.* 2001;44:3710–3720.
- Owen SC, Doak AK, Wassam P, Shoichet MS, Schoichet BK. *Colloidal. ACS Chem. Biol.* 2012;7:1429–1435.
- Budihas SR, Gorshkova I, Gaidamakov S, et al. *Nucleic Acids Res.* 2005;33:1249–1256.
- Maga G, Radi M, Zanoli S, et al. *Angew. Chem. Int. Ed.* 2007;46:1810–1813.
- Radi M, Falciani C, Contemori L, et al. *ChemMedChem.* 2008;3:573–593.
- Klumpp K, Hang JQ, Rajendran S, Yang Y, Derosier A, Wong Kai In, P.; Overton, H.; Parkes, K. E. B.; Cammack, N.; Martin, J. A. *Nucleic Acids Res.* 2003;31:6852–6859.
- Gardelli, C.; Giuliano, C.; Harper, S.; Koch, U.; Narjes, F.; Ontoria, O. J. M.; Poma, M.; Ponzi, S.; Stansfield, I.; Summa, V. WO 2002/06246 A1.
- Molander GA, Canturk B, Kennedy LE. *J. Org. Chem.* 2009;74:973–980.
- Leung CY, Park J, De Schutter JW, Sebag M, Berghuis AM, Tsantrizos YS. *J Med Chem.* 2013;56:7939–7950.
- Agrawal A, DeSoto J, Fullagar JL, et al. *Proc. Natl. Acad. Sci.* 2012;109:2251–2256.
- Zhang D, Ai J, Liang Z, et al. *Bioorg Med Chem.* 2012;20:5169–5180.
- Debenham, JS.; Madsen-Duggan, CB.; Walsh, TF. WO 2008/121257 A1.
- Sun Z, Wang H, Wen K, Li Y, Fan E. *J Org Chem.* 2011;76:4149–4153.
- Le Grice SJ, Grüninger-Leitch F. *Eur J Biochem.* 1990;187:307–314.